The Influence of Polymer Molecular Weight in Lamellar Gels Based on PEG-Lipids

Heidi E. Warriner,* S. L. Keller,# Stefan H. J. Idziak,* Nelle L. Slack,* Patrick Davidson,* Joseph A. Zasadzinski,# and Cyrus R. Safinya*

*Materials Research Laboratory, Materials Department and Physics Department, Biochemistry and Molecular Biology Program, University of California, Santa Barbara, California 93106, and #Chemical and Materials Engineering Department, University of California, Santa Barbara, California 93106 USA

ABSTRACT We report x-ray scattering, rheological, and freeze-fracture and polarizing microscopy studies of a liquid crystalline hydrogel called $L_{\alpha,g}$. The hydrogel, found in DMPC, pentanol, water, and PEG-DMPE mixtures, differs from traditional hydrogels, which require high MW polymer, are disordered, and gel only at polymer concentrations exceeding an "overlap" concentration. In contrast, the $L_{\alpha,g}$ uses very low-molecular-weight polymer-lipids (1212, 2689, and 5817 g/mole), shows lamellar order, and requires a lower PEG-DMPE concentration to gel as water concentration increases. Significantly, the $L_{\alpha,g}$ contains fluid membranes, unlike $L_{\beta'}$ gels, which gel via chain ordering. A recent model of gelation in L_α phases predicts that polymer-lipids both promote and stabilize defects; these defects, resisting shear in all directions, then produce elasticity. We compare our observations to this model, with particular attention to the dependence of gelation on the PEG MW used. We also use x-ray lineshape analysis of scattering from samples spanning the fluid-gel transition to obtain the elasticity coefficients κ and B; this analysis demonstrates that although B in particular depends strongly on PEG-DMPE concentration, gelation is uncorrelated to changes in membrane elasticity.

INTRODUCTION

A gel can be defined as any material that displays both the elastic properties of a solid and the viscosity of a liquid. In biotechnological applications, high-molecular-weight poly(ethylene oxide) [(PEO, $(OCH_2CH_2)_N$)], which has a low immunogenicity, is a standard coating for more immunogenic tissues and materials (Lee, 1991; Peppas and Langer, 1994). Recent studies show that attaching low-molecular-weight ($N < 150$) PEO [poly(ethylene glycol) or PEG] to a biological macromolecule can also substantially increase blood circulation times. In particular, "stealth" liposomes, membrane sacks consisting of closed bilayer shells of phospholipids covered with PEG-lipids hydrophobically anchored to the membrane, show promise as a drug carrier system (Allen and Chonn, 1987; Lasic, 1993; Lasic and Martin, 1995; Lasic and Papahadjopoulos, 1995). These results suggest that PEG-lipids might be useful as a new material in the growing biotechnology industry.

The inhibition of the body's immune response to PEG-coated liposomes has been attributed to a polymer-brush steric repulsion between PEG-coated membranes and the antigenic molecules found in the bloodstream (Alexander, 1977; DeGennes, 1980; Lasic and Martin, 1995). This repulsion has been measured between PEG-coated membranes in the chain-frozen phase (Kuhl et al., 1994) and in the chain-melted fluid phase in multilamellar L_α systems (Kenworthy et al., 1995; Needham et al., 1992). In these systems, PEG-lipids were incorporated into very stiff membranes (bending rigidity $\kappa \geq k_BT$) with intermembrane distances $d \leq R_g$, where R_g is the PEG radius of gyration.

The present work concentrates on a different regime: extremely flexible membranes in a multilamellar L_α system for which $d \gg R_g$. Separated by water, these membranes contain the zwitterionic lipid DMPC, pentanol, and either 0–45 mol % PEG550-DMPE, 0–25 mol % PEG2000-DMPE, or 0–25 mol % PEG5000-DMPE (polyethylene glycol of MW 576, 2053, or 5181 g/mole covalently attached to the headgroup of the zwitterionic lipid DMPE). The chemical structure and molecular weight information for these molecules is summarized in the table of Fig. 1. These membranes are always in the chain-melted fluid state, permitting the polymer-lipid to diffuse or aggregate within the plane of the membrane (Fig. 1). Previous x-ray diffraction work has shown that membranes composed of DMPC and pentanol alone have a very low bending rigidity ($\kappa \sim k_BT$), swelling via the Helfrich undulation repulsion to intermembrane separations >200 Å (Safinya et al., 1989). We show that the addition of PEG-DMPE to these undulation-stabilized membranes extends the stability of the lamellar phase to even larger separations. At low water concentrations, mixtures possess the rheological properties of a fluid

Received for publication 9 September 1997 and in final form 12 March 1998.

Address reprint requests to Dr. Cyrus Safinya, Materials Dept., University of California, MRL Bldg., Room 2208, Santa Barbara, CA 93106. Tel.: 805-893-8635; Fax: 805-893-7221; E-mail: safinya@engineering.ucsb.edu.

Stefan H. J. Idziak's permanent address is Department of Physics, University of Waterloo, Waterloo, Ontario N2L 3G1, Canada.

Patrick Davidson's permanent address is Laboratoire de Physique des Solides (CNRS), Bat. 510, Universite Paris Sud, 91405 Orsay, Cedex, France.

Heidi E. Warriner's permanent address is Lujan Scattering Center, Los Alamos National Laboratory, Los Alamos, New Mexico.

0006-3495/98/07/272/22 $2.00

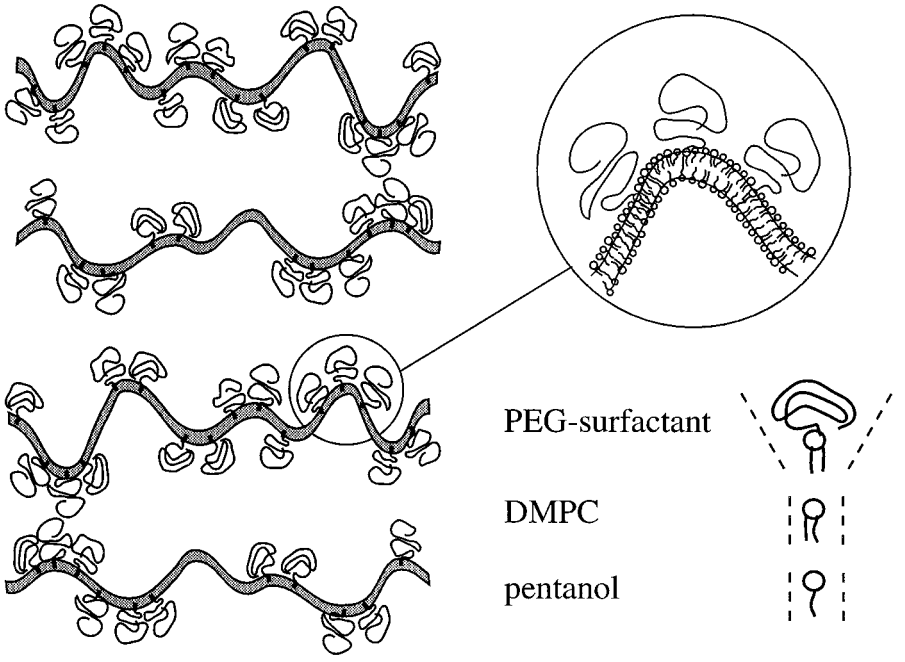

FIGURE 1 Schematic of two undulating membranes composed of DMPC, pentanol, and PEG-DMPE. The membranes are in the fluid state, thus all components are free to diffuse within the plane of the membrane. In the lower right, the non-zero spontaneous curvature of the PEG-DMPE molecule is emphasized in comparison with that of DMPC and pentanol. In the table, the polymerization number *N*, PEG molecular weight, and total molecular weight are summarized for each of the three PEG-DMPE molecules.

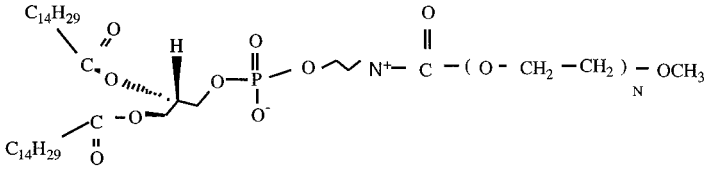

	PEG550	PEG2000	PEG5000
N	13	45	113
PEG MW (Total MW) g/mole	576 (1212)	2053 (2689)	5181 (5817)

but at higher water concentrations a lamellar hydrogel phase forms, hereafter called $L_{\alpha,g}$. The gel appears whether brine or water is used to swell the membranes, indicating that gel formation is not an electrostatic phenomenon. Polarized light and freeze fracture electron microscopy of the $L_{\alpha,g}$ reveals a significant increase in spherulitic and layer dislocation defects that resist both temperature and shear annealing (Keller et al., 1997). X-ray data from powder samples confirm the lamellar structure of the L_α and $L_{\alpha,g}$ phases, but indicate a significant decrease in the domain size of gel samples compared to fluid samples, consistent with an increased defect density. We infer that PEG-DMPE, added to flexible membranes, significantly increases the membrane spontaneous curvature, leading to the proliferation and stabilization of curved regions (defects).

An earlier work (Warriner et al., 1996) presented preliminary results on lamellar hydrogels induced by the addition of PEG2000 and PEG5000 to a highly dilute, flexible, L_α phase. A model for the formation of the $L_{\alpha,g}$ was proposed, based on the idea that PEG-DMPE stabilizes layer dislocation defects by aggregating to regions of high membrane curvature, creating an effective 3-D structure with gel-like elasticity. In a later study of four other PEG-surfactants, it was shown that the hydrophobic moiety of the PEG-surfactant used is not a key factor in the gelation transition (Warriner, 1997; Warriner et al., 1997). In this paper, we present more complete phase diagrams for PEG2000 and PEG5000, as well as the first data for the smaller PEG550. We compare these experimental phase diagrams to the model cited above in terms of 1) the inverse relationship between the intermembrane separation d and both PEG-DMPE concentration and polymer molecular weight at the transition, and 2) the effect of polymer molecular weight on the L_α-$L_{\alpha,g}$ transition. Within the framework of this model we estimate κ, the effective bending rigidity of the polymer-coated bilayers.

In addition, we report the first quantitative fits to small-angle x-ray scattering from polymer-decorated L_α phases.

From these fits, we estimate the value for the single membrane bending rigidity κ and the bulk compressional modulus B as a function of both water and PEG-DMPE concentration. Within the limits of error for this technique, we find that membrane bending rigidity is unaffected for polymer-lipid coverages below a monolayer. We also find that the κ value obtained through the fits agrees well with that extracted from the gelation model. Lastly, our analysis shows that the addition of PEG-DMPE to flexible lamellae leads to a strongly enhanced intermembrane repulsion which is not described either by the Helfrich undulation theory or a polymer mushroom-brush model. However, we demonstrate that this enhanced repulsion is actually only incidental to the L_α-$L_{\alpha,g}$ transition.

MATERIALS AND METHODS

Materials

PEG-DMPEs consisting of dimyristoylphosphatidylethanolamine (MW 635.86) with PEG covalently attached to the amine group (1,2-dimyristoyl-*sn*-glycero-3-phosphoethanolamine-*N*-(poly[ethylene glycol]) were purchased and used without further purification from Avanti Polar Lipids (Alabaster, AL). The three PEG-DMPEs used in our experiments contained PEGs with average molecular weights of 576, 2053, and 5181 g/mole (N = 13, 45, and 113) as summarized in the table of Fig. 1. They are referred to individually as PEG550, PEG2000, and PEG5000, respectively; in discussing them collectively we use the term PEG-DMPE.

Dimyristoylphosphatidylcholine (DMPC) and didodecyldimethyl ammonium bromide (DDAB) were also purchased from Avanti Polar Lipids; pentanol (99% purity) was purchased from Sigma Chemical Corp. (St. Louis, MO). Purified 18 MΩ water was obtained via a Milli-Q Plus unit (Millipore Corp., Bedford, MA). Molecular weights of all membrane components were DMPC, 677.94 g/mole; PEG550, 1212 g/mole; PEG2000, 2689 g/mole; PEG5000, 5817 g/mole; pentanol, 88.15 g/mole. Densities used in all calculations were DMPC and lipid moiety of PEG-DMPE, $\rho_{\text{lipid}} = 1.1$ g/cc (Small, 1986; Trauble and Haynes, 1971); polymer moiety of PEG-DMPE in solution with water, $\rho_{H_2O+PEG} = 1.03$ g/cc (Gonzalez-Tello et al., 1994); pentanol, $\rho_{\text{pentanol}} = 0.81$ g/cc; water in 0 mol % samples, $\rho_{H_2O} = 1.0$ g/cc. Headgroup areas were estimated in the manner described in the Definitions part of the Materials and Methods section and the Phase diagram part of the Results section: for lipids, the headgroup area A_{lipid} was found to be 72.8 ± 0.1 Å^2; for pentanol, the headgroup area A_{pent} was 12.7 ± 0.1 Å^2.

Sample preparations

All samples were prepared in 13-mm diameter glass test tubes. The tubes were first cleaned with a 2:1 vol/vol chloroform/methanol solution, rinsed once with spectroscopic grade ethanol, multiple times with Millipore water, and dried in an oven.

Samples were made with a molar ratio of pentanol to lipid molecules of 4.0 ± 0.5. A high ratio of cosurfactant to surfactant was used to ensure that the lipid chains would always be in the melted state and that the multilayers formed would be sufficiently flexible to display a large undulation repulsion. We also wished to fix the pentanol-to-lipid ratio in order to isolate the effect of PEG-DMPE on membrane fluidity, bending rigidity, and shape. With this ratio fixed, the two remaining compositional degrees of freedom are water content Φ_W (water weight fraction) and the molar ratio of PEG-DMPE to total lipid molecules, c_{PEG} (expressed in %).

Samples were prepared by weighing in the appropriate amounts of lipid, pentanol, PEG-DMPE, and water. Pentanol was always added last, and the test tube top was wrapped in Teflon tape to prevent evaporation. Samples were centrifuged to collect all material at the bottom of the tube and then subjected to ~1/2 h of sonication to break up any clumping. After mixing with a Vortexer (Fisher Scientific, Tustin, CA) the samples were centrifuged again and left to stand for 1–4 weeks before phase determination. After the initial phase determination, samples were checked for any changes every few months.

For a "line" of increasing water samples we often made one large, low water content "seed" sample. After thorough mixing and at least a week of equilibration time, this sample would be "split" into the desired number of samples and the appropriate amount of water added to each new sample to achieve the needed water concentrations. This procedure was most successfully followed for seed samples with "low" PEG lipid concentrations (i.e., $c_{\text{PEG}} < c_{\text{gel}}$ for the seed water amount) because the long equilibration time for highly viscous samples made it difficult to verify that gel seed samples were at equilibrium. In cases where we used a gel seed sample to create an increasing water line, we spot-checked our results with "singly made" samples along the same line.

Definitions and formulas

Phase diagrams for all PEG-DMPEs were constructed both in terms of weight fraction water versus mol % PEG-DMPE (Φ_W vs. c_{PEG}), and intermembrane spacing d versus volume fraction of PEG-DMPE in the bilayer membrane, $\Phi_{\text{mem}_{\text{PEG}}}$. The time and expense required for rheological tests on more than 400 samples were prohibitive, thus to construct phase diagrams we adopted the following "operational" definition of a gel: any sample that does not flow for at least 5 s after inversion of the test tube. In the two series of samples for which we did run quantitative rheological tests (described below) we found that gelation occurred somewhat earlier than the concentrations indicated by the above criterion (e.g., at lower Φ_W or lower c_{PEG}). However, a consistent application of this simpler, operational definition results in a phase diagram close to that obtained through more quantitative rheological data.

For each of the three phase diagrams, the relevant definitions given below were used. For all equations, g_x is the weight in grams of material x. In Eqs. 5 and 7, the factor of $1 - g_{H_2O}(0.026/0.974)$ multiplying the pentanol volume takes into account the 2.6 w/w % solubility of pentanol in water (Stephen and Stephen, 1963–1979).

$$d = \frac{2\pi}{q_0} \tag{1}$$

where q_0 is the peak position of the first harmonic in the x-ray diffraction pattern

$$\delta d = \frac{d^2 \cdot (\text{stepsize in x-ray scan})}{\pi} \tag{2}$$

$$\Phi_w = \frac{g_{\text{water}}}{g_{\text{total}}} \tag{3}$$

$$c_{\text{PEG}} = 100 \cdot \left(\frac{g_{\text{PEG-LIPID}}/MW_{\text{PEG-LIPID}}}{g_{\text{PEG-LIPID}}/MW_{\text{PEG-LIPID}} + g_{\text{DMPC}}/MW_{\text{DMPC}}} \right) \tag{4}$$

$$\Phi_{\text{mem}_{\text{PEG}}} = \left(1 + \frac{\left(\frac{g_{\text{DMPC}}}{\rho_{\text{DMPC}}} + \frac{g_{\text{pentanol}}}{\rho_{\text{pentanol}}} \times \left(1 - g_{H_2O}\left(\frac{.026}{.974} \right) \right) \right)}{\left(\frac{g_{\text{PEG-LIPID}}}{\text{MW}_{\text{PEG-LIPID}}} \right) \times \left(\frac{\text{MW}_{\text{PEG-LIPID}}}{\rho_{H_2O+PEG}} + \frac{\text{MW}_{\text{DMPE}}}{\rho_{\text{DMPE}}} \right)} \right)^{-1} \tag{5}$$

We also use the classical relationship between the intermembrane spacing d and the volume fraction of membrane Φ_{mem} to find δ, the bilayer thickness:

$$\delta = d \times \Phi_{mem} \tag{6}$$

where

$$\Phi_{mem} = \left(\frac{1 + \frac{\frac{g_{pentanol}}{\rho_{pentanol}} \times \left(1 - g_{H_2O}\left(\frac{0.026}{0.974}\right)\right)}{\frac{g_{PEG\text{-}lipid}}{\rho_{lipid}} \times \left(\left(\frac{MW_{DMPE}}{MW_{PEG\text{-}lipid}}\right) + g_{DMPC}\right)}}{1 + \frac{\frac{g_{pentanol}}{\rho_{pentanol}} + \left(\frac{g_{PEG\text{-}lipid} \times \left(\frac{MW_{PEG}}{MW_{PEG\text{-}lipid}}\right) + g_{H_2O}}{\rho_{H_2O+PEG}}\right)}{\frac{g_{PEG\text{-}lipid}}{\rho_{lipid}} \times \left(\left(\frac{MW_{DMPE}}{MW_{PEG\text{-}lipid}}\right) + g_{DMPC}\right)}} \right) \tag{7}$$

In Eq. 5, the volume fraction of PEG-DMPE in the bilayer includes the polyethylene glycol moiety of the polymer-surfactant as part of the bilayer, while in Eq. 7 the polymer part of PEG-DMPE is excluded from the calculation of the volume fraction of the membrane. This paradox results from the dual nature of PEG-DMPE: 1) it acts to swell the intermembrane distance like an equivalent volume of solvent and so must be counted as part of the solvent in Eq. 7, but 2) the effective headgroup-to-chain area ratio of PEG-DMPE surfactant is controlled by the size of the polymer moiety (Fig. 1); hence, this part of the polymer-lipid must be taken into account in calculations relating to average bilayer properties or composition.

We determine the area per headgroup for the molecules in the membrane using standard relationships between area and volume for a predominately flat membrane. Taking the areas of the DMPC and bare DMPE headgroups to be approximately equal, we calculate the average headgroup area per lipid:

$$\langle A_{mem} \rangle = V_{mem}/\delta N_{mem} \text{ and}$$

$$V_{mem} = \frac{(g_{PEG\text{-}lipid} \times (MW_{DMPE}/MW_{PEG\text{-}lipid}) + g_{DMPC})}{\rho_{lipid}}$$

$$+ \frac{g_{pentanol}}{\rho_{pentanol}} \times (1 - g_{H_2O}(0.026/0.974)) \tag{8}$$

where V_{mem} is the volume of sample occupied by the membrane and

$$\langle A_{mem} \rangle = \frac{N_{LIPID}}{N_{mem}}(\langle A_{LIPID} \rangle - \langle A_{pentanol} \rangle) + \langle A_{pentanol} \rangle \tag{9}$$

Equation 9 has the form of a straight line with intercept equal to the headgroup area of pentanol and slope given by the difference between the lipid and alcohol headgroup areas. Here N_{mem} is the total number of molecules in the membrane after the water solution is saturated with pentanol.

X-ray diffraction

X-ray scattering studies were performed in-house using an 18 kW Rigaku rotating anode generator (Rigaku, Danvers, MA) (CuK_α, $\lambda = 1.54$ Å), a cylindrically bent focusing pyrolitic graphite (002) monochromator and a Bicron point detector (Bicron, Newbury, OH). The in-plane resolution, defined using slits, had a FWHM = 0.01–0.015 $Å^{-1}$ and the out-of-plane resolution had a FWHM = 0.14–0.3 $Å^{-1}$; scan stepsize was generally 0.001 $Å^{-1}$. Additional experiments were carried out at the Stanford Synchrotron Radiation Laboratory on beamlines 6-2 and 10-2 using either a Bicron point detector or a 180-mm MAR image-plate 2-D x-ray detector (Mar Industries, San Diego, CA). In the Bicron experiments, in-plane resolution, again defined by slits, was FWHM = 0.0014–0.0028 $Å^{-1}$ and the out-of-plane resolution was FWHM = 0.01–0.02 $Å^{-1}$; scan stepsize was usually 0.0005 $Å^{-1}$. For the 2-D detector experiments resolution and stepsize were defined by the detector pixel size and the distance from sample to detector. Images were radially averaged to produce powder scans with a stepsize of 0.0007 $Å^{-1}$ and a radially averaged FWHM of 0.0027 $Å^{-1}$. Exposure times were typically 1–2 h.

Samples were flame-sealed in either quartz or glass 1.5-mm x-ray capillary tubes (Charles Supper Co., Natick, MA). These capillary tubes were then set on a translation stage for automated data acquisition. We found it necessary to heat and quench some of the samples from the fluid regime in order to obtain a proper "powder" form, i.e., an isotropic distribution of lamellar domains.

Rheology

Constant-stress oscillatory shear-strain experiments were carried out with a Rheometrics dynamic stress rheometer, model 1710C (Rheometrics, Piscataway, NJ), in the cone and plate geometry with a 40-mm diameter plate, a cone angle of 0.04 radians, and a gap size of 0.05 mm. During testing, a small housing was placed around the setup which enclosed pentanol and water-soaked cotton balls in order to minimize evaporation.

Samples were subjected to three different tests. The first test was a dynamic stress sweep test in which the stress is increased from ~0.6–100 dynes/cm^2 at a frequency of 1 Hz to establish the regime of linear viscoelasticity. Each sample was then tested in a transient single point test within this regime to ensure the sinusoidal strain response followed the sinusoidal stress by a phase angle. Finally, a dynamic frequency sweep test was run at a constant stress over a frequency range of 0.01–10 Hz to determine both the real (storage elasticity) modulus, G', and the imaginary (loss) modulus, G''. For each sample, two sets of tests were run. The first set included the dynamic stress sweep test, the transient single point test, and the dynamic frequency sweep test. For the second set of tests, a fresh sample from the same test tube was used and only the dynamic frequency sweep test was run in order to check the reproducibility of the first set of tests. In particular, we wished to ensure that the dynamic moduli were not merely products of alignment produced during the high stresses imposed in a dynamic stress sweep test.

Optical microscopy

Optical glass capillaries (Vitro Dynamics, Rockaway, NJ) of thicknesses ranging from 0.05 to 0.2 mm were filled with sample and flame-sealed. Some capillaries were cleaned first with a 2% solution of PCC-54 concentrate (Pierce, Rockford, IL), then rinsed with spectroscopic grade ethanol, rinsed multiple times with Millipore water, dried and then subjected to 30–90 min of UV light in order to heighten the hydrophilicity of the glass, thus increasing the probability of homeotropic alignment. All samples were observed with an Optiphot 2-Pol microscope (Nikon, Torrance, CA) using polarized light at different magnifications (50–500×). Textures were photographed using a MFX-DX automatic camera and posemeter (Nikon, Torrance, CA). The microscope was also equipped with an FP82 heating stage and an FP80 central processor (Mettler-Toledo Inc., Hightstown, NJ) for temperature annealing experiments.

Freeze-fracture electron microscopy

Freeze-fracture electron microscopy was performed as in Chiruvolu et al. (1994), and the replicas processed as in Fetter and Costello (1986) except that replicas were bathed in ethanol and retrieved on formvar coated microscopy grids. Samples were imaged in a TEM JEOL100CX at an accelerating voltage of 100 keV.

RESULTS

Phase diagrams

In this section we show that the addition of any of the PEG-DMPEs to a phase of undulation-stabilized membranes promotes the formation of a lamellar hydrogel phase, labeled $L_{\alpha,g}$. This hydrogel is distinct from entanglement-based polymeric gels in that it forms only at high water concentrations. Counterintuitively, at low water concentrations where the polymer-lipid concentration is necessarily higher, mixtures possess the rheological properties of a fluid. We also show that PEG-DMPE actually tends to stabilize the lamellar phase, permitting dilution to larger intermembrane separations than are achievable for L_α phases composed of bare membranes.

To eliminate the effect a changing cosurfactant/surfactant ratio exerts on viscoelastic properties, all samples used in this paper were made with a pentanol-to-lipid molar ratio of 4.0 ± 0.5 (Fig. 2 *A*). However, due to the non-zero solubility of pentanol in water (Stephen and Stephen, 1963–1979), the actual amount of pentanol retained in the membrane decreases with increasing water concentration, yielding an actual intramembrane pentanol-to-lipid ratio of ~3.0 ± 1.5, samples of higher water concentration having the lowest ratios. However, this higher effective variation in intramembrane pentanol concentration is not the source of the dramatic increase in viscoelasticity between the two lamellar regimes: high water samples made without PEG-DMPE do not gel. When the partial solubility of pentanol is taken into account, a plot of the lamellar period versus membrane volume fraction shows the linear behavior of a 1-D lamellar system (Fig. 2 *B*). Both the L_α and $L_{\alpha,g}$ regimes for all the PEG-DMPEs are well described by a bilayer thickness of 27.8 ± 0.1 Å separated by a solvent composed of water, PEG, and trace amounts of dissolved pentanol (Fig. 2 *B*). Since the membrane thickness is independent of c_{PEG}, this is the thickness of the bare (no polymer) membrane. This value for the membrane thickness is in excellent agreement with earlier values for DMPC-pentanol membranes of ~28 Å (Safinya et al., 1989).

Noting that the average headgroup area per membrane molecule $\langle A_{mem}\rangle$ is a weighted average between the lipid and pentanol molecules, we use the variation in the intramembrane pentanol concentration to calculate the average headgroup area for each type of molecule. In Fig. 2 *C*, where $\langle A_{mem}\rangle$ is plotted versus the number fraction of lipid molecules in the membrane, an unweighted, straight-line fit yields a value for $\langle A_{LIPID}\rangle$ of 72.8 ± 0.1 Å^2, and for $\langle A_{pentanol}\rangle$ of 12.7 ± 0.1 Å^2, consistent with previous headgroup area measurements from phosphocholine bilayers in the L_α phase (Reiss-Husson, 1967; Small, 1986) and DMPC/pentanol solutions (Safinya, personal communication, 1995).

Fig. 3 shows the phase diagrams of the PEG-DMPEs as a function of weight fraction water (Φ_{water}) and mol % PEG-DMPE (c_{PEG}), while Fig. 4 gives the same information

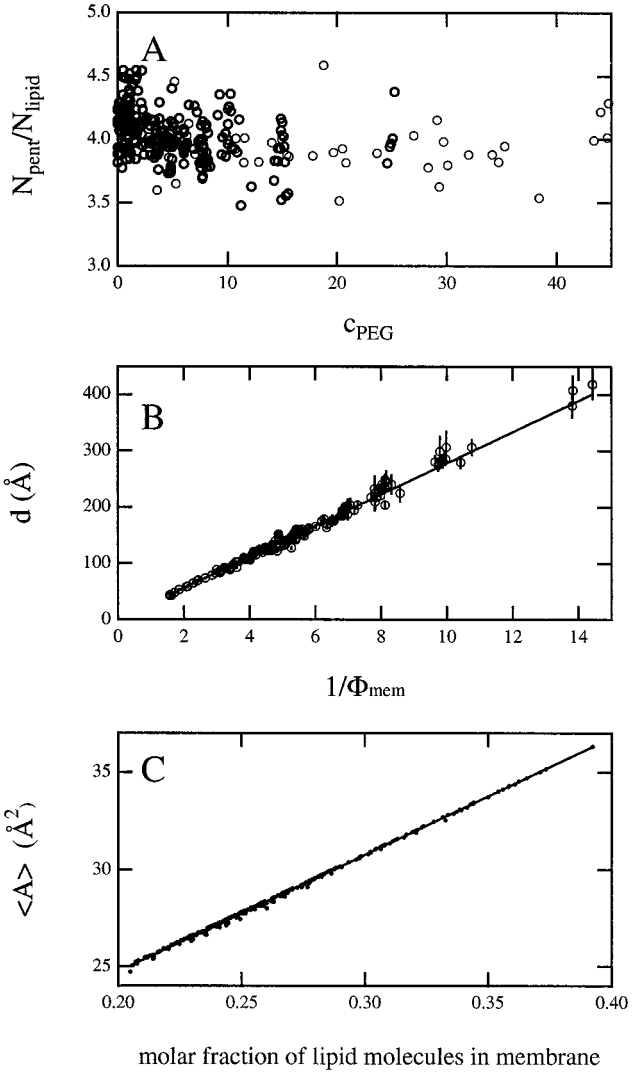

FIGURE 2 (*A*) Pentanol-to-lipid molar ratio as a function of c_{PEG} for all PEG550, PEG2000, and PEG5000 mixtures used in this paper. This ratio of 4.0 ± 0.5 is the calculated ratio based on the relative amounts of pentanol and lipid weighed into the sample and does not reflect the partial solubility of pentanol in water. When this partial solubility is taken into account, the intramembrane molar ratio is 3.0 ± 1.5, still a small enough variation not to significantly alter the sample viscoelasticity. (*B*) Intermembrane distance *d* versus $1/\Phi_{mem}$ (membrane volume fraction of the sample) for all single-phase PEG550, PEG2000, and PEG5000 samples. Regardless of viscoelasticity, polymer-lipid concentration, or polymer molecular weight, the membrane thickness δ is stable at 27.8 ± 0.1 Å. The fit is to Eq. 6 with error bars given by Eq. 2; reduced χ^2 was 1.91 for 174 points. (*C*) Average area per intramembrane molecule $\langle A_{mem}\rangle$ versus the molar fraction of lipid molecules in the membrane. Physically, $\langle A_{mem}\rangle$ is a weighted average of the headgroup areas of the lipid and pentanol molecules; the partial solubility of pentanol in water forces this average to vary in a systematic way. We use this variation as described in the Materials and Methods section to obtain an average lipid headgroup area A_{lipid} of 72.8 ± 0.1 Å and an average pentanol headgroup area of 12.7 ± 0.1 Å. Values are from an unweighted fit to Eq. 9; χ^2 was 1.67 for 314 points.

in terms of the intermembrane spacing *d* and the membrane volume fraction of PEG-DMPE ($\Phi_{mem_{PEG}}$). From Fig. 3 *B*, mixtures with low $c_{PEG2000}$ and $\Phi_W \leq 0.42$ are two-phase. These samples, when viewed in the bulk after moderate

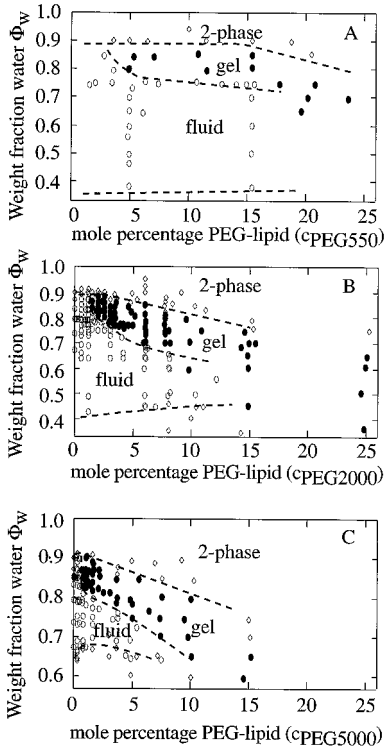

FIGURE 3 Phase diagrams of the PEG550, PEG2000, and PEG5000 systems in terms of weight fraction water (Φ_W) and mol % PEG-lipid (c_{PEG}). Open circles represent fluids, solid circles represent gels, and diamonds represent two-phase samples. The dotted lines between the fluid and gel regimes are intended to guide the eye. (*A*) PEG550. Note that the lamellar system is not stable for $\Phi_W \geq 0.33$. (*B*) PEG2000. The lamellar system is not stable for $\Phi_W \geq 0.42$. (*C*) PEG5000. The lamellar system is not stable for $\Phi_W \geq 0.66$. For all the PEG-DMPEs there is an inverse relationship between the amount of water required to achieve gelation and the concentration of PEG-lipid.

centrifugation, show a clear meniscus between an isotropic and a birefringent phase; consistent with this, the small angle x-ray scattering contains both an isotropic liquid peak and lamellar diffraction peaks (data not shown). This boundary corresponds to an intermembrane spacing d of ~53 Å (Fig. 4 *B*) or a fluid spacing d_w ($= d-\delta$) of 25 Å. The radius of gyration R_g for PEG2000 incorporated in lipid bilayers has been measured to be 25–35 Å (Kuhl et al., 1994), matching the location of this lower two-phase boundary. This behavior is replicated in both the PEG550 and PEG5000 phase diagrams; in Fig. 3, *A* and *C*, the lower two-phase boundary occurs at Φ_W ~0.33 and Φ_W ~0.66, respectively, corresponding to fluid spacings of ~16 and 63 Å. By using Flory scaling arguments one can extrapolate the PEG2000 R_g measurement to the other two PEG-DMPEs, obtaining a value for the PEG550 R_g of ~15 Å and for the PEG5000 R_g of ~60 Å. We surmise, therefore, that the PEG-DMPE lamellar regime is stable only when the fluid spacing d_W is large enough to accommodate a swollen polymer coil. Thus the position of the lower two-phase boundary in this type of phase diagram is a simple and accurate method of determining the average polymer extension from a bilayer.

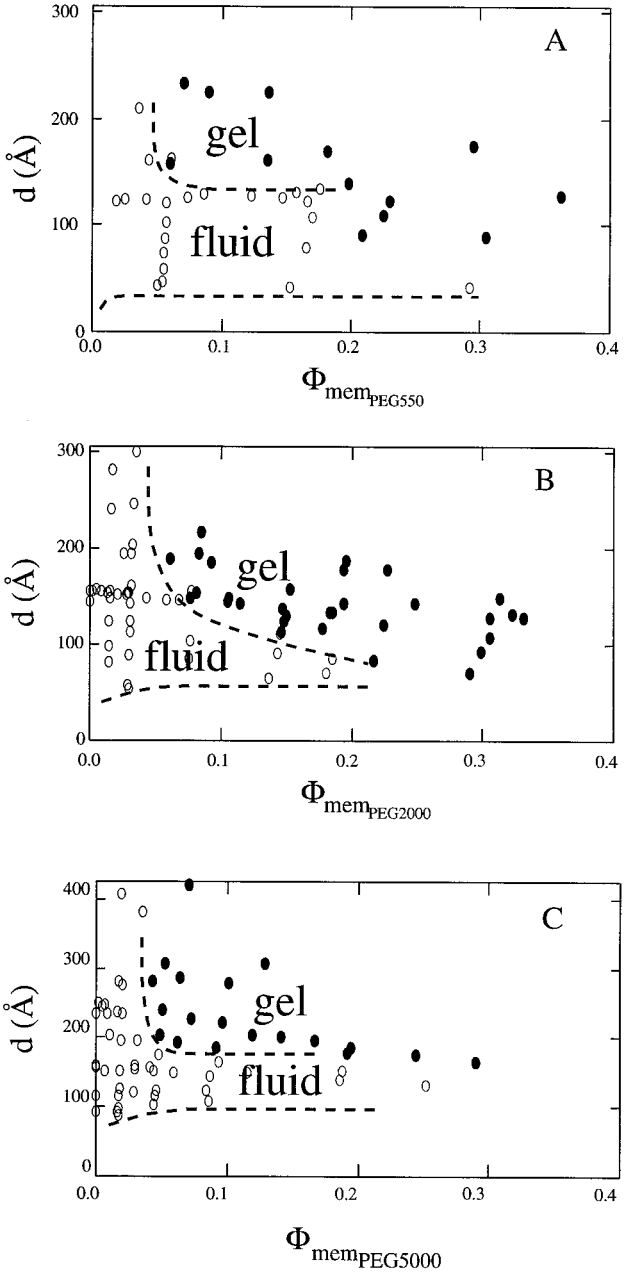

FIGURE 4 Phase diagrams of the PEG550, PEG2000, and PEG5000 systems in terms of intermembrane spacing d and the volume fraction of the membrane occupied by the PEG-DMPE molecules, $\Phi_{mem_{PEG}}$. Open circles represent fluids, solid circles represent gels. The dotted lines between the fluid, gel, and two-phase regimes are intended as guides to the eye. (*A*) PEG550. The lamellar system is not stable for spacings below 42 Å or $d_w < 14$ Å, close to the calculated polymer R_g of 17 Å. (*B*) PEG2000. The lamellar system is not stable for spacings below 53 Å or $d_w < 25$ Å, consistent with the measured polymer R_g of 25–35 Å. (*C*) PEG5000. The lamellar system is not stable for spacings below 91 Å or $d_w \geq 63$ Å, approximately the calculated polymer R_g of 60 Å. For all the PEG-DMPEs the intermembrane spacing at which gelation occurs is inversely proportional to the concentration of PEG-DMPE.

Above this lower two-phase boundary, two lamellar regimes with remarkably different viscoelastic and optical properties are observed. These differences are qualitatively

demonstrated in Fig. 5. The lower water concentration lamellar regime, which we refer to simply as L_α, possesses the rheological properties of a low-viscosity fluid (Fig. 5 *A*, bottom two samples). The $L_{\alpha,g}$ regime, accessed from the L_α through the addition of either PEG-DMPE or water, retains the lamellar microstructure of the L_α samples but exhibits a strong gel-like elasticity (e.g., Fig. 5 *A*, third sample from the bottom). A simple demonstration of this elasticity is the ability to maintain nonspherical shapes for indefinite periods (Fig. 5 *B*). Viewed between crossed polarizers, an L_α sample will typically exhibit a uniformly bright, somewhat flat appearance, free of macroscopic features (Fig. 5 *C*). In contrast, $L_{\alpha,g}$ samples are generally less birefringent than L_α samples and, when viewed between crossed polarizers in bulk, display macroscopic features reminiscent of the nematic Schlieren texture (Fig. 5 *D*) (Demus and Richter, 1978; Gray and Goodby, 1984).

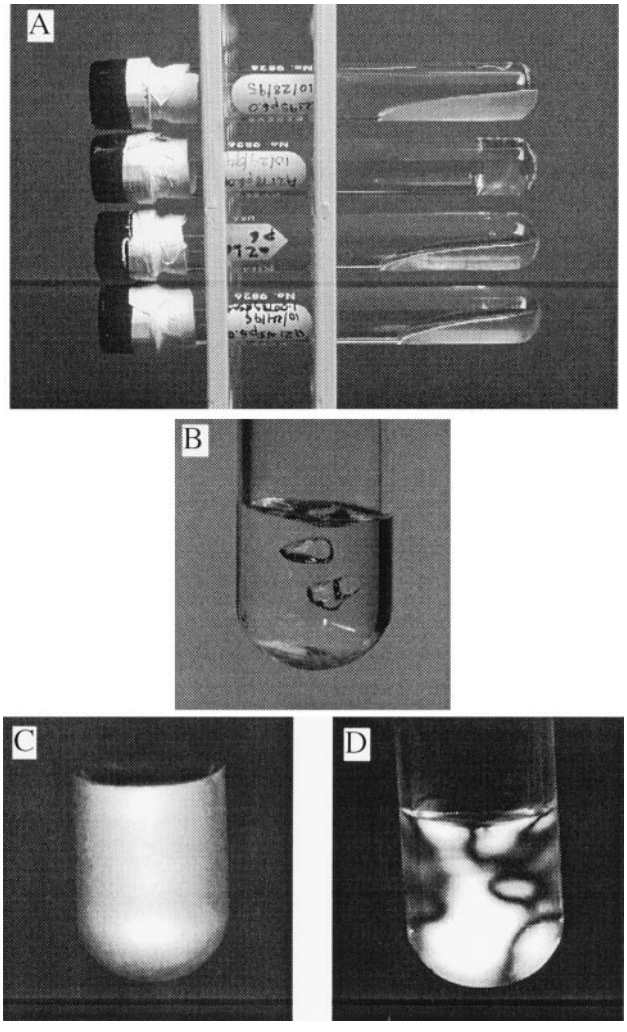

FIGURE 5 (*A*) Four samples with $c_{PEG2000} \cong 6$ mol % and, from bottom to top, increasing water concentration illustrate the fluid-to-gel to two-phase transitions. From bottom to top: fluid sample with $\Phi_{water} = 0.45$ ($d = 55$ fluid sample with $\Phi_{water} = 0.68$ ($d = 110$ Å); gel sample with $\Phi_{water} = 0.78$ ($d = 165$ two-phase sample with $\Phi_{water} = 0.95$. (*B*) Fluid sample with $c_{PEG2000} = 1.2$, $\Phi_{water} = 0.49$ between crossed polarizers. The uniformly bright, somewhat flat appearance of this sample is typical of low-water fluid samples. Fluid samples of higher water content are similarly devoid of macroscopic features, but may be more colorful. (*C*) Gel sample with $c_{PEG2000} = 6.0$, $\Phi_{water} = 0.85$ between crossed polarizers. Macroscopic liquid crystalline defects have replaced the featureless appearance of the fluid sample. (*D*) Gel sample with $c_{PEG2000} = 6.0$, $\Phi_{water} = 0.79$ showing nonspherical bubbles. The ability to maintain arbitrary shapes against surface tension is a qualitative demonstration of elastic properties.

The transition between these two lamellar regimes is fairly broad; average widths in terms of Φ_W are ± 0.03 and in c_{PEG}, ± 0.5 mol %. At low PEG-DMPE concentrations, the transition curve in the three phase diagrams of Fig. 3 is roughly

$$\Phi_w \propto \frac{1}{c_{PEG}} \tag{10}$$

or, in Fig. 4,

$$d \propto \frac{1}{\Phi_{mem_{PEG}}} \tag{11}$$

That is, less PEG-DMPE is required to gel mixtures of higher water concentration. This general behavior immediately differentiates the $L_{\alpha,g}$ from free polymer hydrogels in which the polymer concentration must exceed c*, the polymer mushroom overlap concentration, in order for entanglement and gelation to occur. Remarkably, the $L_{\alpha,g}$ occurs at polymer and water concentrations that preclude the possibility of direct polymer interactions as a gelation mechanism. The $L_{\alpha,g}$ is found in 1 mol % PEG5000 mixtures with measured fluid spacings of ~400 Å (Fig. 4 *C* and Warriner, 1997); in the PEG550 and PEG2000 systems, d_w of a gel approaches 200 Å (Fig. 4, *A* and *B* and Warriner, 1997). These separations are many times greater than the polymer R_g.

Lateral interactions, in particular the mushroom-brush transition (Alexander, 1977; DeGennes, 1976), are also irrelevant in the L_α-$L_{\alpha,g}$ transition. Using our values for the lipid and pentanol headgroup areas, one can calculate the expected monolayer coverage for these membranes, i.e., the PEG-DMPE concentration c_{mono} at which the polymer "mushrooms" would first begin to overlap and interact:

$$\begin{aligned}\text{total area} = 72.8\ \text{Å}^2 \times \left(\frac{g_{\text{PEG-DMPE}}}{\text{MW}_{\text{PEG-DMPE}}} + \frac{g_{\text{DMPC}}}{\text{MW}_{\text{DMPC}}}\right) \\ + 12.7\ \text{Å}^2 \times \left(\frac{g_{\text{pent}}}{\text{MW}_{\text{pent}}}\right) \approx 118\ \text{Å}^2 \\ \times \left(\frac{g_{\text{PEG-DMPE}}}{\text{MW}_{\text{PEG-DMPE}}} + \frac{g_{\text{DMPC}}}{\text{MW}_{\text{DMPC}}}\right)\end{aligned} \tag{12}$$

and

$$\frac{\text{area}}{\text{mushroom}} = R_g^2 \times \left(\frac{g_{\text{PEG-DMPE}}}{\text{MW}_{\text{PEG-DMPE}}}\right) \tag{13}$$

Equating 12 and 13 gives

$$c_{mono} \approx \frac{118}{R_g^2} \tag{14}$$

For PEG550, c_{mono} is ~40 mol %; for PEG2000, ~10 mol %; for PEG5000, ~3 mol %. From Fig. 3, the $L_{\alpha,g}$ begins at concentrations up to eight times less than c_{mono}. Moreover, gel samples have been prepared using a 0.5 M NaCl solution in place of water, ruling out long-range electrostatic interactions in gel formation.

The upper two-phase boundary has the same general shape in all the phase diagrams of Fig. 3, decreasing from $\Phi_W \cong 0.85–0.90$ at low c_{PEG} to $\Phi_W \cong 0.70–0.73$ at the highest PEG concentrations studied. However, as demonstrated in Fig. 4, the position of the upper two-phase boundary in terms of intermembrane spacing depends strongly on the molecular weight of the polymer lipid used. This effect is explained by recalling that the polymer moiety of the PEG-DMPEs add to the intermembrane spacing in the same way as an equivalent volume of water. Thus PEG5000 samples are actually stable up to intermembrane spacing $d > 400$ Å, whereas the highest measured spacing for a single-phase sample in the PEG2000 system approaches only 300 Å, and in the PEG550 sample the highest measured spacing is just over 200 Å. Samples just beyond the upper two-phase boundary appear to be composed of a lamellar phase plus excess water; however, no detailed study of this regime has been undertaken.

Rheology

Quantitative rheological tests were performed on 10 PEG2000 samples. Five samples had $c_{PEG2000}$ fixed at 6 mol % with the weight fraction of water Φ_W increasing from 0.45 to 0.79; the other five had a nearly constant *d*-spacing (140 Å ± 15 Å) with $c_{PEG2000}$ increasing from 1.73 to 15.36 mol %. For all samples, at least two measurements of the real (elasticity) modulus G' and the imaginary (loss, viscosity) modulus G'' were made as described in the Introduction. For the purposes of this section, samples showing gel-like elastic behavior are those for which G' is reliably greater than G'' over the full range of frequencies measured. We compare this definition to the one used in the phase diagrams of the previous section.

The evaluation of G' and G'' demonstrates the strong elasticity of samples from the gel regime. Fig. 6 shows data taken as a function of frequency (dynamic frequency sweep test) on the line of increasing water samples after a dynamic stress sweep test was performed. For the two lowest Φ_W samples (Fig. 6, *A* and *B*), the elastic and viscous components of the dynamic moduli are comparable with G'/G'' ~2–3. These samples were classified as fluids in the phase diagram; consistent with that determination, rheological data from such samples tended to be less reproducible than data from gel samples. For example, in Fig. 7 *A*, two sets of frequency data for a sample classified as fluid taken before and after a dynamic stress sweep test are plotted. Although the data were taken at the same constant stress with the same volume of sample, the moduli differ by almost an order of magnitude between the tests. In other experiments,

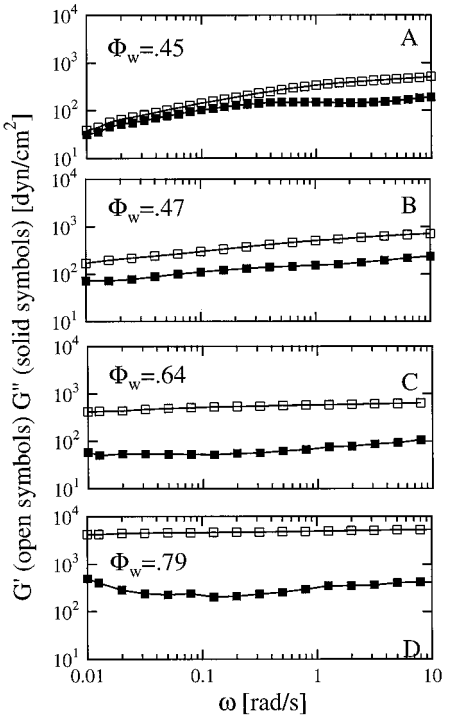

FIGURE 6 Rheological data from four samples with $c_{PEG2000} \cong 6$ mol % but increasing water concentration. Open symbols are G', the elasticity modulus and closed symbols show G'', the viscosity modulus. Note the strong increase in the elastic character of the samples as the water concentration increases and the samples change from fluids to gels. (*A*) Fluid sample, $\Phi_{water} = 0.45$, $G'/G'' \sim 2–3$. (*B*) Fluid sample, $\Phi_{water} = 0.47$, $G'/G'' \sim 2–3$. (*C*) Sample approaching the transition region, $\Phi_{water} = 0.64$, $G'/G'' \sim 10$. Although the G', G'' measurement indicates this material is a gel, it flows under its own weight before 5 s elapse, and so was classified a fluid in the phase diagrams. (*D*) Gel sample, $\Phi_{water} = 0.79$, $G'/G'' \sim 13$.

a crossover frequency (frequency at which the elastic and viscous moduli are equal) was observed in samples after a dynamic stress sweep test was run but was not seen in the same sample if a dynamic stress sweep test was not run. This phenomenon is explained by noting fluids have no shear resistance. That is, during shear, liquid crystalline samples with the viscoelastic properties of a fluid can realign, altering the measured response (Lu and Cates, 1994; Safinya, et al., 1993). Gels, on the other hand, resist shear, yielding a reproducible response; in Fig. 7 *B* frequency data for a gel sample before and after a dynamic stress sweep test are essentially unchanged.

Between the $\Phi_W = 0.47$ and $\Phi_W = 0.64$ samples, elasticity values increase markedly; for $\Phi_W = 0.79$ the elastic portion of the dynamic moduli has increased by more than an order of magnitude from the $\Phi_W = 0.47$ value. Similar results are obtained as a function of increasing PEG-DMPE concentration. In Fig. 8, G' grows by two orders of magnitude as c_{PEG} increases from 1.73 to 15.36 mol %. Although both the viscosity and elasticity moduli increase between the fluid and gel samples, the elasticity gains are consistently greater: in both lines of samples the ratio of G' over G'' grows by an order of magnitude over initial (fluid) values.

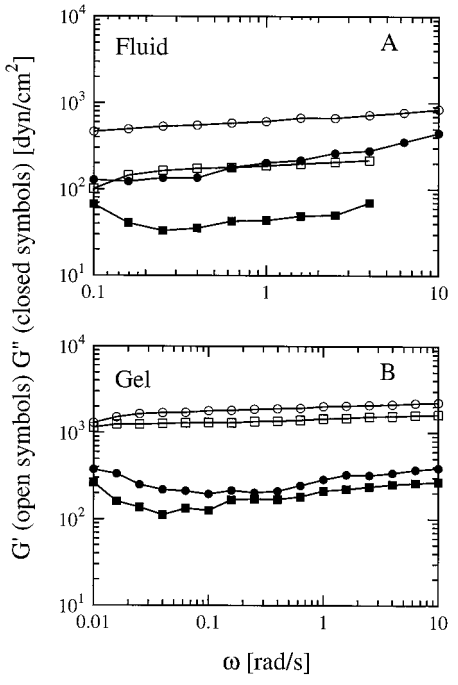

FIGURE 7 Typical data from a fluid and a gel sample before (*circles*) and after (*squares*) the dynamic stress sweep test (DSST), which subjects the sample to large stresses (up to 100 dynes/cm^2) in order to determine the limits of linear viscoelasticity. Open symbols are G', the elasticity modulus, while closed symbols show G'', the viscosity modulus. (*A*) Fluid sample with $c_{PEG} = 6.0$, $\Phi_{water} \cong 0.49$. The sample realigned during the DSST, producing much lower values for both viscoelastic moduli in the second test. (*B*) Gel sample with $c_{PEG} = 3.76$, $\Phi_{water} \cong 0.77$. Gels, unlike fluids, can resist the high shears imposed in the DSST, yielding a consistent response.

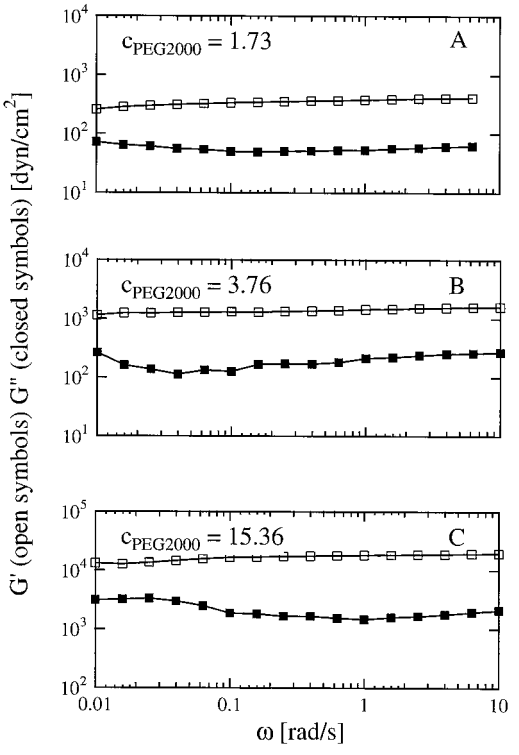

FIGURE 8 Rheological data of three samples with $\Phi_{water} \cong 0.77$ demonstrates that augmenting sample c_{PEG} leads to gelation as readily as increasing Φ_{water}. Open symbols are G', the elasticity modulus, while closed symbols show G'', the viscosity modulus. (*A*) Sample near the transition region, $c_{PEG2000} = 1.73$, $G'/G'' \sim 4$. Although the G', G'' measurement indicates this material is a gel, it flows under its own weight before 5 s elapse, and so was classified a fluid in the phase diagrams. (*B*) Gel sample, $c_{PEG2000} = 3.76$, $G'/G'' \sim 6$. (*C*) Gel sample, $c_{PEG2000} = 15.36$, $G'/G'' \sim 10$.

From Fig. 6 we would surmise that the L_α-$L_{\alpha,g}$ transition at 6 mol % PEG2000 occurs between $\Phi_W = 0.47$ and $\Phi_W = 0.64$, instead of the ~0.70 indicated in the phase diagram. Similarly, from Fig. 8, the transition for $\Phi_W = 0.78$ occurs before 1.73 mol % instead of at 2.0 mol %, as shown in Fig. 3 *B*. The discrepancy arises from the use of an "operational" 5-s inversion test to classify samples for the phase diagram: i.e., only samples with yield stresses greater than their own weight (as tested by inverting the samples for 5 s and checking for flow) were classified as gels. Under this definition, some gels will be classified as fluids; however, no fluids will be classified as gels. Thus, the 5-s definition delays identification of the L_α-$L_{\alpha,g}$ transition in terms of c_{PEG} or Φ_W from the concentrations indicated by quantitative rheologic data, and makes it impossible to attribute particular significance to absolute values of c_{PEG} and Φ_W at the transition. However, the key, intriguing observation of this study is unaltered by the choice of definition of gelation: for all PEG-DMPE's, the concentration of PEG-DMPE required for gelation is inversely proportional to the water content. Moreover, the arguments employed in the previous section to eliminate polymer entanglement and long-range electrostatic interactions as gelation mechanisms also remain valid regardless of which definition of gelation is used.

X-ray diffraction

Figs. 9 and 10 show small-angle synchrotron x-ray data obtained from unoriented, i.e., "powder," PEG2000 and PEG5000 samples (data for PEG550 are comparable). For the scans in Fig. 9, Φ_W was kept constant to within ± 0.05 while c_{PEG} increased from 0 to just above 15 mol % (PEG2000) or from 0 to 6 mol % (PEG5000). For the scans shown in Fig. 10, c_{PEG} was fixed at the indicated value while Φ_W increased. The spectra are almost evenly split between samples from the gel and fluid regimes. Regardless of PEG-DMPE molecular weight or concentration, water concentration or viscoelastic properties, the samples display lamellar diffraction patterns and are well-described by a bilayer of 27.8 ± 0.1 Å separated by a solvent composed of PEG, water, and trace amounts of pentanol (Fig. 2 *B*). Additionally, scans of the interference peak at 1.4 Å^{-1} show that the lipid chain interactions remains liquid-like regardless of macroscopic viscoelasticity (Fig. 11). Thus the addition of PEG-DMPE to a flexible L_α phase dramatically increases bulk viscoelasticity without altering either the local lamellar symmetry or diminishing membrane fluidity. In particular, unlike $L_{\beta'}$ gels, chain-ordering is not the source of gelation.

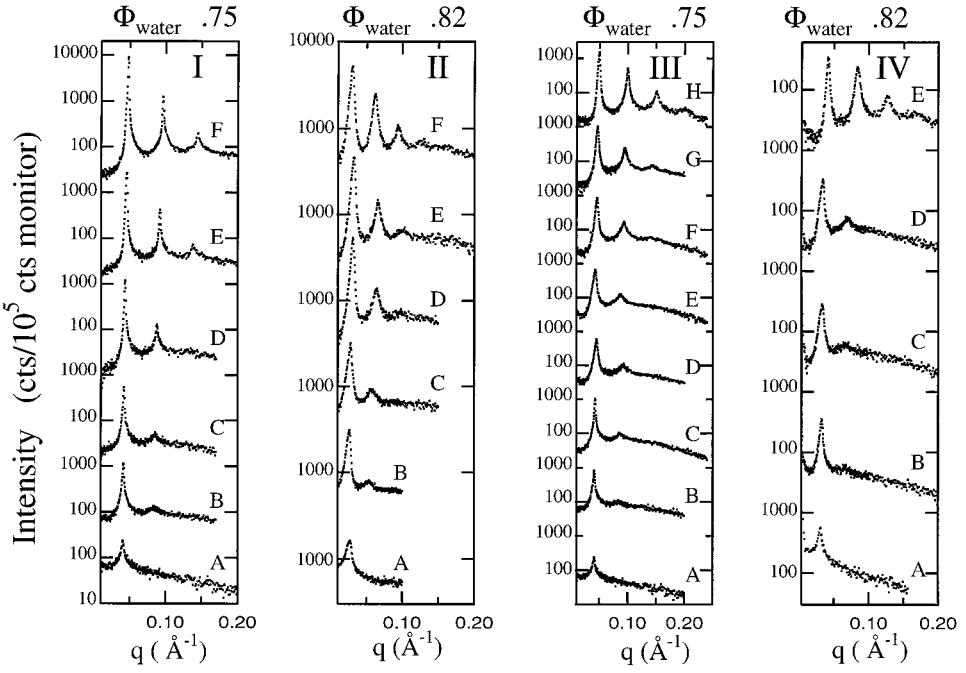

FIGURE 9 Synchrotron x-ray scattering data as a function of increasing c_{PEG} for PEG5000 (I, *A–F* and II, *A–F*) and PEG2000 (III, *A–H*, IV, *A–E*) samples. (I) Moderate water content samples from the fluid L_α regime of PEG5000. (*A*) $c_{PEG5000} = 0$, $\Phi_w = 0.79$, $d = 153$ Å. (*B*) $c_{PEG5000} = 0.50$, $\Phi_w = 0.79$, $d = 153$ Å. (*C*) $c_{PEG5000} = 0.76$, $\Phi_w = 0.79$, $d = 152$ Å. (*D*) $c_{PEG5000} = 1.60$, $\Phi_w = 0.77$, $d = 145$ Å. (*E*) $c_{PEG5000} = 3.79$, $\Phi_w = 0.75$, $d = 140$ Å. (*F*) $c_{PEG5000} = 5.43$, $\Phi_w = 0.72$, $d = 132$ Å. (II) High water content samples drawn equally from the fluid and gel regimes of PEG5000. (*A*) Fluid, $c_{PEG5000} = 0$, $\Phi_w = 0.85$, $d = 234$ Å. (*B*) Fluid, $c_{PEG5000} = 0.25$, $\Phi_w = 0.85$, $d = 238$ Å. (*C*) Fluid, $c_{PEG5000} = 1.17$, $\Phi_w = 0.84$, $d = 227$ Å. (*D*) Gel, $c_{PEG5000} = 2.09$, $\Phi_w = 0.82$, $d = 204$ Å. (*E*) Gel, $c_{PEG5000} = 3.12$, $\Phi_w = 0.81$, $d = 195$ Å. (*F*) Gel, $c_{PEG5000} = 5.95$, $\Phi_w = 0.79$, $d = 207$ Å. (III) Samples of moderate water content drawn equally from the fluid and gel regimes of PEG2000. (*A*) Fluid, $c_{PEG2000} = 0$, $\Phi_w = 0.79$, $d = 157$ Å. (*B*) Fluid, $c_{PEG2000} = 1.09$, $\Phi_w = 0.79$, $d = 153$ Å. (*C*) Fluid, $c_{PEG2000} = 2.9$, $\Phi_w = 0.78$, $d = 147$ Å. (*D*) Fluid, $c_{PEG2000} = 3.54$, $\Phi_w = 0.77$, $d = 137$ Å. (*E*) Gel, $c_{PEG2000}$ 4.2, $\Phi_w = 0.77$, $d = 147$ Å. (*F*) Gel, $c_{PEG2000} = 6.01$, $\Phi_w = 0.76$, $d = 137$ Å. (*G*) Gel, $c_{PEG2000} = 7.8$, $\Phi_w = 0.75$, $d = 133$ Å. (*H*) Gel, $c_{PEG2000} = 15.6$, $\Phi_w = 0.70$, $d = 127$ Å. (IV) Samples of high water content drawn equally from the fluid and gel regimes of PEG2000. (*A*) Fluid, $c_{PEG2000} = 0$, $\Phi_w = 0.83$, $d = 202$ Å. (*B*) Fluid, $c_{PEG2000} = 0.91$, $\Phi_w = 0.83$, $d = 195$ Å. (*C*) Gel, $c_{PEG2000} = 2.19$, $\Phi_w = 0.82$, $d = 189$ Å. (*D*) Gel, $c_{PEG2000} = 3.44$, $\Phi_w = 0.82$, $d = 184$ Å. (*E*) Gel, $c_{PEG2000} = 15.32$, $\Phi_w = 0.76$, $d = 151$ Å. The number of harmonics, and hence the intermembrane repulsion, is a strong function of the PEG-lipid concentration. However, this repulsion is unconnected to the fluid-gel transition as evidenced by I, *A–F*, where the number of harmonics steadily increases but the samples retain the viscoelastic response of fluids.

Examining Figs. 9 and 10 in more detail, some general trends become apparent. First, the number of harmonics present in a spectrum is an increasing function of the PEG-DMPE concentration, but basically independent of Φ_W. Second, the shape (asymmetry, slope) of the x-ray peaks is also strongly affected by the presence of PEG-DMPE. Third, peaks from gel samples are generally broader than those from fluid samples. Previous theoretical (Caille, 1972; Gunther et al., 1980; Lei et al., 1995) and experimental work on stacked membrane systems (Als-Nielsen et al., 1980; Keller et al., 1991; Safinya, 1989) has demonstrated that changes in the x-ray lineshape reveal changes in material parameters and interactions. In particular, the Caille structure factor, originally developed to describe diffraction from smectic A liquid crystals (Caille, 1972), has been successfully extended to describe scattering from electrostatically (Roux and Safinya, 1988) and undulation-stabilized L_α systems (Helfrich, 1978; Safinya, 1989; Safinya et al., 1986, 1989) and from the smectic A phase of polymeric liquid crystals (Keller et al., 1991). Here, we apply the Caille theory to a system of polymer-coated, chain-melted, flexible, stacked lamellae.

Although the Caille theory has been extensively tested for undulation-stabilized systems (Roux and Safinya, 1988; Safinya, 1989; Safinya et al., 1986, 1989), this is the first application we are aware of to flexible membranes containing end-anchored polymers. Thus, there is no existing evidence that the Landau-DeGennes Hamiltonian correctly describes the interactions between lamellae of this type of material. There is no prior work to show that the Helfrich undulation repulsion (Helfrich, 1978), which is the dominant interaction between uncharged, flexible membranes, remains important for flexible membranes carrying a polymer coat. We should therefore first explicitly examine the general agreement among the Caille structure factor, the Helfrich theory, and the observed scattering before using these models to probe the relationship between microscopic parameters, interactions, and trends in the bulk viscoelasticity.

Brief review of the Caille x-ray lineshape and Helfrich undulation repulsion

The Caille theory relates the x-ray lineshape to the intermembrane spacing *d*, bulk compressional modulus B, and

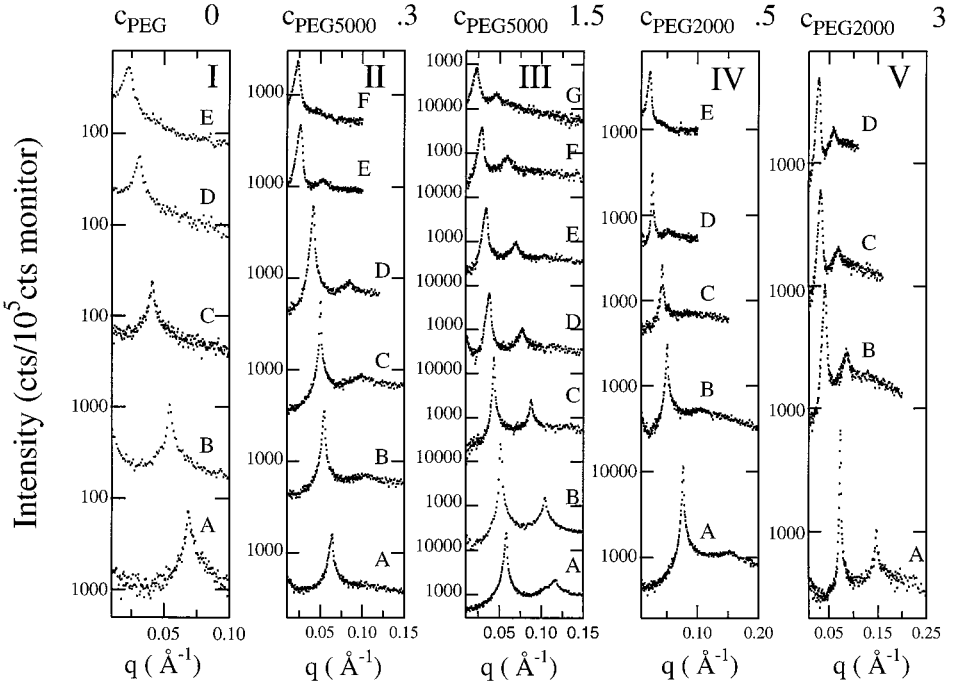

FIGURE 10 Synchrotron x-ray scattering data as a function of increasing water for samples without PEG-lipid (I, *A–E*), and for PEG5000 (II, *A–F* and III, *A–G*) and PEG2000 (IV, *A–E*, V, *A–E*) samples. (I) All samples are in the fluid L_α regime with $c_{PEG} = 0$. (*A*) $\Phi_w = 0.67$, $d = 92$ Å. (*B*) $\Phi_w = 0.74$, $d = 117$ Å. (*C*) $\Phi_w = 0.79$, $d = 153$ Å. (*D*) $\Phi_w = 0.83$, $d = 202$ Å. (*E*) $\Phi_w = 0.87$, $d = 282$ Å. (II) All samples are in the fluid L_α regime. (*A*) $c_{PEG5000} = 0.31$, $\Phi_w = 0.69$, $d = 98$ Å. (*B*) $c_{PEG5000} = 0.31$, $\Phi_w = 0.73$, $d = 115$ Å. (*C*) $c_{PEG5000} = 0.31$, $\Phi_w = 0.75$, $d = 126$ Å. (*D*) $c_{PEG5000} = 0.31$, $\Phi_w = 0.79$, $d = 152$ Å. (*E*) $c_{PEG5000} = 0.25$, $\Phi_w = 0.85$, $d = 238$ Å. (*F*) $c_{PEG5000} = 0.31$, $\Phi_w = 0.87$, $d = 274$ Å. (III) PEG5000 samples drawn equally from the fluid and gel regimes. (*A*) Fluid, $c_{PEG5000} = 1.61$, $\Phi_w = 0.70$, $d = 109$ Å. (*B*) Fluid, $c_{PEG5000} = 1.62$, $\Phi_w = 0.73$, $d = 122$ Å. (*C*) Fluid, $c_{PEG5000} = 1.60$, $\Phi_w = 0.77$, $d = 145$ Å. (*D*) Fluid, $c_{PEG5000} = 1.65$, $\Phi_w = 0.80$, $d = 165$ Å. (*E*) Gel, $c_{PEG5000} = 1.59$, $\Phi_w = 0.82$, $d = 184$ Å. (*F*) Gel, $c_{PEG5000} = 1.60$, $\Phi_w = 0.84$, $d = 220$ Å. (*G*) Gel, $c_{PEG5000} = 1.67$, $\Phi_w = 0.87$, $d = 279$ Å. (IV) All samples are from the fluid regime of PEG2000. (*A*) $c_{PEG2000} = 0.55$, $\Phi_w = 0.64$, $d = 82$ Å. (*B*) $c_{PEG2000} = 0.55$, $\Phi_w = 0.75$, $d = 125$ Å. (*C*) $c_{PEG2000} = 0.56$, $\Phi_w = 0.79$, $d = 149$ Å. (*D*) $c_{PEG2000} = 0.55$, $\Phi_w = 0.85$, $d = 241$ Å. (*E*) $c_{PEG2000} = 0.55$, $\Phi_w = 0.87$, $d = 281$ Å. (V) PEG2000 samples drawn equally from the fluid and gel regimes. (*A*) Fluid, $c_{PEG2000} = 3.0$, $\Phi_w = 0.64$, $d = 85$ Å. (*B*) Fluid, $c_{PEG2000} = 3.0$, $\Phi_w = 0.79$, $d = 153$ Å. (*C*) Gel, $c_{PEG2000} = 3.0$, $\Phi_w = 0.82$, $d = 193$ Å. (*D*) Gel, $c_{PEG2000} = 3.0$, $\Phi_w = 0.84$, $d = 217$ Å. All samples, regardless of viscoelasticity, display a lamellar diffraction pattern. Although gelation occurs readily upon increasing Φ_w, the number and strength of harmonics seems relatively unaffected by water content, i.e., by intermembrane distance.

bulk bending elasticity K. Analysis of two series of samples spanning the L_α-$L_{\alpha,g}$ transition, one in the direction of increasing Φ_W, the other in the direction of increasing c_{PEG}, offers an opportunity to examine material constants (K, *d*) and interactions (B) in light of the increase in bulk viscoelasticity. The Caille theory begins with the Landau-De Gennes expression for the energy density of a smectic A liquid crystal.

$$\frac{F}{V} = \frac{1}{2}\left\{B\left(\frac{du}{dz}\right)^2 + K\left(\frac{d^2u}{dx^2} + \frac{d^2u}{dy^2}\right)^2\right\} \tag{15}$$

Here u(**r**) is the layer displacement in the *z* direction normal to the layers. Landau and Peierls (Landau, 1965) first showed that for this Hamiltonian, thermally induced mean square layer displacements diverge logarithmically with the domain size *L*, destroying long-range order. In this case, conventional delta-function Bragg peaks are replaced by power law divergences (Caille, 1972). For a powder sample, profiles of the (00*l*) reflections have the asymptotic form (Roux and Safinya, 1988; Safinya et al., 1986)

$$S(q) \approx |q - q_{00l}|^{1-\eta_l} \quad \text{where} \quad \eta_l \equiv \frac{l^2 q_{001}^2 k_B T}{8\pi\sqrt{BK}} \equiv l^2\eta \quad \text{if} \quad \eta_l < 1 \tag{16}$$

If $1 < \eta_l < 2$, this asymptotic form no longer applies. While there is no theoretical limit on η_l, for $\eta_l > 2$, the singularity is replaced by a liquid-like cusp (Safinya, personal communication, 1997) and detection becomes difficult. The observation of a singularity-like (00*l*) reflection requires that the exponent $1 - \eta_l$ be positive; thus a rough estimate of $\eta \propto 1/\sqrt{KB}$ can be made from the number of detected reflections. For example, if only one harmonic is apparent, $\eta \sim 1$; if two are detected, then $\eta \sim 0.25$, etc. From these arguments and Fig. 9, it is clear that as c_{PEG} increases (to 6 mol % for PEG5000 or 15 mol % for PEG2000), η decreases by an order of magnitude. Therefore the product of the microscopic elasticities, (BK), grows by two orders of magnitude. To clearly separate increases in the strength of intermem-

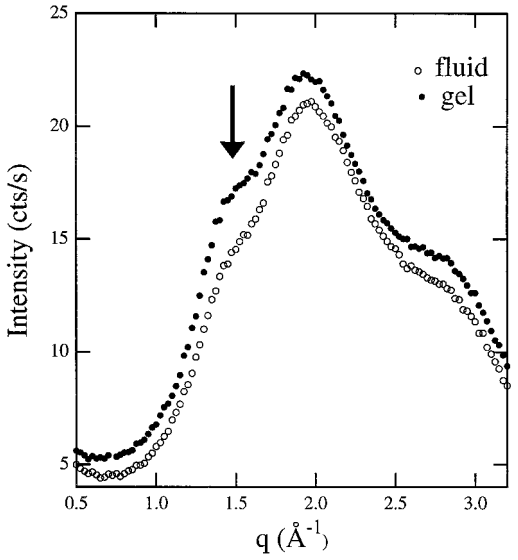

FIGURE 11 Typical high-angle rotating anode data for a PEG2000 fluid (*open circles*) and gel (*closed circles*) displaying the lipid chain-interference peak at 1.5 Å^{-1} (*arrow*) and water peaks at 2 and 2.7 Å^{-1}. Note that for both samples the lipid peak is broad and liquid-like, indicating that intramembrane molecules are free to diffuse regardless of macroscopic sample viscoelasticity.

brane interaction (B) from changes in material rigidity (K) requires a more formal analysis.

Accordingly, the real-space Caille correlation function is given by (Als-Nielsen et al., 1980)

$$G(\mathbf{r}) \propto \left(\frac{1}{\rho}\right)^{2\eta_l} \exp\left(-2\gamma\eta_l - \eta_l E_1\left(\frac{\rho^2}{4\lambda z}\right)\right)$$

where

$$\lambda \equiv \sqrt{\frac{K}{B}}$$

$$\gamma \equiv \text{Euler's constant} \tag{17}$$

$$E_1 \equiv \text{Exponential integral function}$$

In a single crystal of finite size L, the structure factor is the Fourier transform of $G(\mathbf{r})$

$$S(0, 0, q_z) \propto \iiint G(\mathbf{r}) \exp(-\pi r^2/L^2) \exp[-i(q - q_z)\cdot \mathbf{r}] d^3\mathbf{r} \tag{18}$$

For a powder, we explicitly average $S(0, 0, q_z)$ over all solid angles in reciprocal space.

$$S(|q_z|) \equiv \int S(0, 0, q_z) d\Omega_q$$

$$\propto \int_{-\infty}^{\infty} dz \int_0^{\infty} G(z, \rho) \exp(-\pi r^2/L^2) \frac{\sin(qr)}{qr} \exp(-q_{00l} z) d\rho \tag{19}$$

For each harmonic of order l, there are five fitted parameters: η_l, λ, L, q_{00l}, and a prefactor I_l. For a given sample, all harmonics should give the same value of λ and L, but η_l should scale as l^2. From η and λ, B and K are extracted:

$$K \equiv \frac{\kappa}{d} \equiv \frac{q_0^2 \lambda}{8\pi\eta} k_B T \quad \text{or equivalently} \quad \kappa \equiv \frac{q_0 \lambda}{4\eta} k_B T \tag{20}$$

where κ is the bending rigidity of a single membrane

$$B \equiv 1.64 \cdot 10^9 \left(\frac{q_0^2}{\eta\lambda}\right) \text{ergs/cm}^3 \tag{21}$$

In Eq. 19, the in-plane resolution is implicit in the finite size term $\exp(-\pi r^2/L^2)$. If $\exp(-q_z^2/\sigma_z^2)$ is the in-plane resolution, the true domain size L_{true} is extracted from the fitted parameter L by

$$L_{true} = \sqrt{\frac{4\pi}{\sqrt{\left(\frac{4\pi}{L}\right) - (\sigma_z^2)}}} \tag{22}$$

However, the out-of-plane resolution $\exp(-q_\rho^2/\sigma_\rho^2)$ must be explicitly convolved with the calculated $S(q)$. Since λ and σ_ρ can oppositely affect the peak asymmetry, this step in the analysis is *extremely* important. Out-of-plane resolution effects, also called axial divergence, tend to broaden the low-q side of small-angle peaks, while a small λ (large compressional modulus B) will increase peak asymmetry by steepening the low-q side. In the absence of a proper treatment of the out-of-plane resolution, it is not possible to correctly determine λ. To a lesser degree, values for η and L will also be compromised in an attempt to compensate for the improperly handled peak asymmetry.

While the above is essentially a technical difficulty, there are also more intrinsic limitations to the use of lineshape analysis. For larger values of λ ($\sim$20 Å), or, equivalently, smaller B ($\sim 10^7$ ergs/cm^3), the "true" peak shape will be fairly symmetric, and thus insensitive to the λ parameter. In this case values of B and K or κ derived via lineshape analysis are correspondingly less certain than in the case of small λ (large B).

In Caille's argument, the interaction between membranes that gives rise to B and K is not specified; any interaction that can be described by the Landau-Degennes Hamiltonian (Eq. 15) will give rise to a Caille lineshape. The Helfrich undulation repulsion, which obeys Eq. 15, specifies that steric hindrance between adjacent membranes is the dominant interaction. In a multilayer system this gives rise to a repulsive pressure given by

$$P = \frac{3\pi^2}{64} \frac{(k_B T)^2}{\kappa} \frac{1}{(d - \delta)^3} \tag{23}$$

where δ is the membrane thickness

It follows specifically that

$$\mathrm{B} \equiv -V\frac{\partial P}{\partial V} = \frac{9\pi^2}{64}\frac{(k_\mathrm{B}T)^2}{\kappa}\frac{d}{(d-\delta)^4} \text{ at constant membrane area} \tag{24}$$

Thus B, in the Helfrich model, is inversely proportional to both the repeat spacing d and the membrane bending rigidity κ.

Membrane elasticity and interactions as a function of intermembrane distance and polymer-lipid concentration

Fits of the Caille lineshape (Eq. 19) to all harmonics for four samples of increasing (top to bottom) c_{PEG2000} are shown in the semi-log plots of Fig. 12. Peaks have been centered at $q = 0$ by subtracting the peak position q_{00l} from the actual wave numbers. For all samples, $\Phi_\mathrm{W} \sim 0.75$; these are the same spectra shown without fits in Fig. 9, III*A*, *C*, *G*, and *H*. The Caille profile clearly replicates the observed scattering very well; reflecting this, reduced χ^2 values are typically between 1 and 2, close to the ideal value of 1. In particular, for all PEG-DMPE concentrations, successive harmonics yield fairly constant values for λ and domain size, and show the l^2 scaling behavior for η expected for a material governed by the Landau-DeGennes Hamiltonian. In Fig. 13, the fit-derived values of L, λ, and η, along with the Caille-predicted scaling for ηl, are shown for the four harmonics of the spectrum of Fig. 12 *D* or 9, III*H*. We conclude that the Landau-DeGennes Hamiltonian, and hence the Caille structure factor, correctly describe this material, and can be used to find B, K, and the domain size L.

However, the Helfrich model is not applicable. Fig. 14 shows plots of the fit-derived parameters λ, η, B, and κ for a line of increasing c_{PEG2000} samples with $\Phi_\mathrm{W} \sim 0.75$ and $d = 140 \pm 15$ Å. Spectra for the majority of these samples are shown in Fig. 9, III. The dotted line shows the position of the L_α-$L_{\alpha,\mathrm{g}}$ transition for these samples. It is immediately clear from the plots of Fig. 14, *C* and *D* that B is not inversely proportional to κ, as required for Helfrich undulation repulsion (Eq. 24). As c_{PEG2000} increases from 0 to 8 mol %, κ is constant to within the precision of our measurements, while B grows by almost a factor of 15. In fact, growth in κ is detectable only after the mushroom-brush point while most of the increase in B happens before c_{mono} ($\sim$10 mol %). Thus, while there seems to be a strong connection between membrane bending elasticity and grafted polymer conformation, the intermembrane repulsion between these *flexible*, fluid, polymer-decorated layers is not connected to the mushroom-brush transition. Moreover, the fluid spacing d is 3–4 times R_g, too large for a mushroom force to be effective. Preliminary work indicates that the stiffened compressibility is due to an undulation-induced antidepletion interaction originating from the freely diffusing PEG chains anchored at the fluid membrane interface (Warriner et al., in preparation).

However, this increased repulsion does not correlate with the appearance of the $L_{\alpha,\mathrm{g}}$ phase. In Fig. 15 we show plots of λ, η, B, and κ for a line of samples with increasing Φ_W and $c_{\mathrm{PEG2000}} = 6.05 \pm 0.04$ mol %. Again, the dotted line indicates the L_α-$L_{\alpha,\mathrm{g}}$ transition. From Fig. 15, *C* and *D*, both κ and B *decrease* as we move across the transition, reaching in the gel phase values comparable to those found for fluid L_α samples in the increasing c_{PEG} series of Fig. 14, *C* and *D*. The apparent softening of κ is an approximately logarithmic function of Φ_{mem} ($\sim 1 - \Phi_\mathrm{W}$) and has been predicted for flexible membranes (Helfrich, 1978). We thus eliminate κ and B as agents in the formation of the $L_{\alpha,\mathrm{g}}$. This leaves the domain size, L, as the last material parameter to check for correlations with the L_α-$L_{\alpha,\mathrm{g}}$ transition.

A marked increase in the width of the lamellar peaks from samples in the $L_{\alpha,\mathrm{g}}$ regimes is indeed a distinctive feature of the x-ray spectra. In Fig. 16 we show histograms of first harmonic peak widths from powder samples in the gel and fluid regimes of PEG2000 and PEG5000. The two distributions are strikingly different; a Kolmogorov-Smirnov test gives a $1.6 \cdot 10^{-8}$ probability that the two histograms are actually drawn from the same distribution. In particular, the average of the gel distribution is at least three times larger than that of the fluids (because the average of the fluid distribution is smaller than the resolution used in collecting the data, we can only make a lower bound estimate of the difference between the two). Peak width is inversely proportional to domain size. Since domains are bounded by defected regions, the reduction in domain size connotes an increase in the average defect density between the L_α and $L_{\alpha,\mathrm{g}}$ regimes. We return to this correlation between the appearance of stable defects and the viscoelastic transition in the next section.

Microscopy

Figs. 17 and 18 illustrate characteristic defect textures encountered in polarization and freeze-fracture electron microscopy of L_α and $L_{\alpha,\mathrm{g}}$ samples. In Fig. 17, *A–C* we show typical freeze-fracture textures from a series of three PEG2000 samples of increasing c_{PEG} and constant Φ_W (0.78 ± 0.01) that cross the fluid-to-gel transition; Fig. 17, *E–G* shows optical textures for the same three samples. For comparison, data for a 95% water suspension of DDAB MLVs is shown in Fig. 17, *D* and *H*. Fig. 18 shows polarization photos taken of a series of four PEG5000 samples of fixed c_{PEG} and increasing Φ_W that also cross the fluid to gel transition.

The photos of Fig. 17, *A* and *E* are taken of a sample from the fluid regime. In Fig. 17 *A* we see mostly well-aligned, parallel sheets of lamellae (star), which can extend for many microns. Relatively large spherulitic or MLV defects are also observed (*arrows*). The polarization photos shown of the same sample in Fig. 17 *E* and of a PEG5000 L_α sample

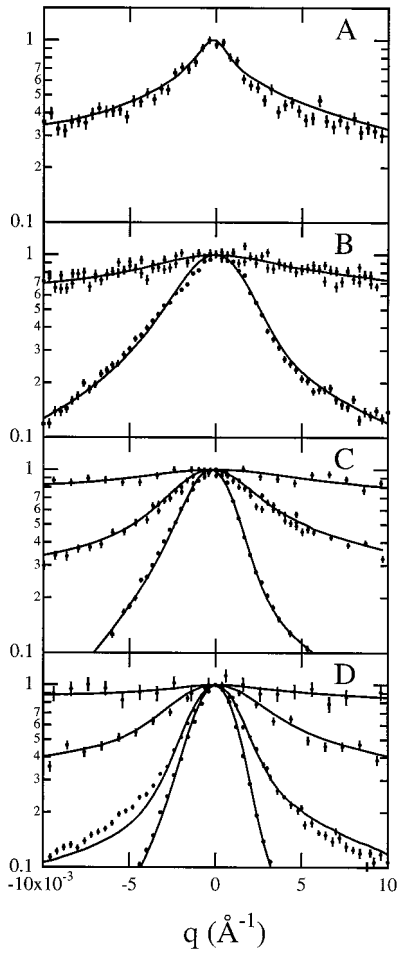

FIGURE 12 Fits to all harmonics for four samples of increasing (*top* to *bottom*) $c_{PEG2000}$. Peaks and fits have been normalized to unity and also centered at $q = 0$ by subtracting the peak position q_l from the measured q. The solid lines are independent fits to each harmonic by the Caille power law line shape. (*A*) Fluid sample with one harmonic, $c_{PEG2000} = 0$, $\Phi_w = 0.79$, $d = 153$ Å. From the fit, $\eta = 0.77 \pm 0.02$, $\lambda = 15 \pm 1$, and $q_{001} = 0.0412$ Å^{-1}. From these values, κ is $0.2 \pm 0.02\ k_BT$ and B is $2.3 \pm 0.2 \cdot 10^5$ ergs/cm^3. Peak width for this sample is resolution-limited, hence no determination of domain size can be made. Reduced $\chi^2 = 1.37$. (*B*) Fluid sample showing two harmonics, $c_{PEG2000} = 1.63$, $\Phi_w = 0.78$, $d = 145$ Å. For the first (narrower peak), $\eta = 0.32 \pm 0.01$, $\lambda = 5.8 \pm 1$, and $q_{001} = 0.0432$ Å^{-1}. Peak width is determined by the resolution. Reduced $\chi^2 = 2.2$. For the second broader peak, $\eta_2 = 1.21 \pm 0.03$, $\lambda = 8.5 \pm 1.8$, and $q_{002} = 0.0863$ Å^{-1}. Reduced $\chi^2 = 0.2$. The average η, λ are determined by an unweighted average. Uncertainties were calculated to be the larger of 1) the sigma of the average resulting from the spread in the individual values, or 2) the error derived from a standard application of error propagation formulas to the individual errors. Accordingly, $\eta = 0.31 \pm 0.07$, $\lambda = 7.2 \pm 1.3$. From these values, κ is $0.25 \pm 0.07\ k_BT$ and B is $13 \pm 2 \cdot 10^5$ ergs/cm^3. (*C*) Gel sample showing three harmonics, $c_{PEG2000} = 7.8$, $\Phi_w = 0.75$, $d = 147$ Å. For the first (narrowest peak), $\eta = 0.19 \pm 0.01$, $\lambda = 4.9 \pm 1$, $L = 2300 \pm 100$ Å, and $q_{001} = 0.0475$ Å^{-1}. Reduced $\chi^2 = 2.2$. For the second, broader peak, $\eta_2 = 0.64 \pm 0.01$, $\lambda = 9.5 \pm 1$, $L = 1600 \pm 100$ Å, and $q_{002} = 0.0953$ Å^{-1}. Reduced $\chi^2 = 1.6$. For the last peak, $\eta_3 = 1.09 \pm 0.03$, $\lambda = 9.5 \pm 1.1$, $L = 1100 \pm 200$ Å, and $q_{003} = 0.1434$ Å^{-1}. Reduced $\chi^2 = 1.1$. The average η, λ are $\eta = 0.16 \pm 0.03$, $\lambda = 8.0 \pm 2.0$; κ is therefore $0.6 \pm 0.2\ k_BT$ and B is $28 \pm 9 \cdot 10^5$ ergs/cm^3. (*D*) Gel sample showing three harmonics, $c_{PEG2000} = 15.6$, $\Phi_w = 0.70$, $d = 125$ Å. For the first (narrowest peak), $\eta = 0.12 \pm 0.01$, $\lambda = 11.8 \pm 1$, $L = 2400 \pm 100$ Å, and $q_{001} = 0.0500$ Å^{-1}. Reduced $\chi^2 = 5.2$. For the second, broader peak, $\eta_2 = 0.34 \pm 0.01$, $\lambda = 10.7 \pm 1.2$, $L = 2100 \pm 100$ Å, and $q_{002} = 0.1003$ Å^{-1}. Reduced $\chi^2 = 7.23$. For the third peak, $\eta_3 = 0.65 \pm 0.02$, $\lambda = 10.7 \pm 1.0$, $L = 1400 \pm 100$ Å, and $q_{003} = 0.1508$ Å^{-1}. Reduced $\chi^2 = 1.4$. The fourth, broadest harmonic has $\eta_4 = 1.2 \pm 0.11$, $\lambda = 8.9 \pm 3.2$, $L = 1860 \pm 320$ Å, and $q_{003} = 0.2004$ Å^{-1}. Reduced $\chi^2 = 1.06$. The average η and λ are $\eta = 0.09 \pm 0.02$, $\lambda = 10.5 \pm 1.0$; $\kappa = 1.5 \pm 0.3\ k_BT$ and B is $44 \pm 10 \cdot 10^5$ ergs/cm^3.

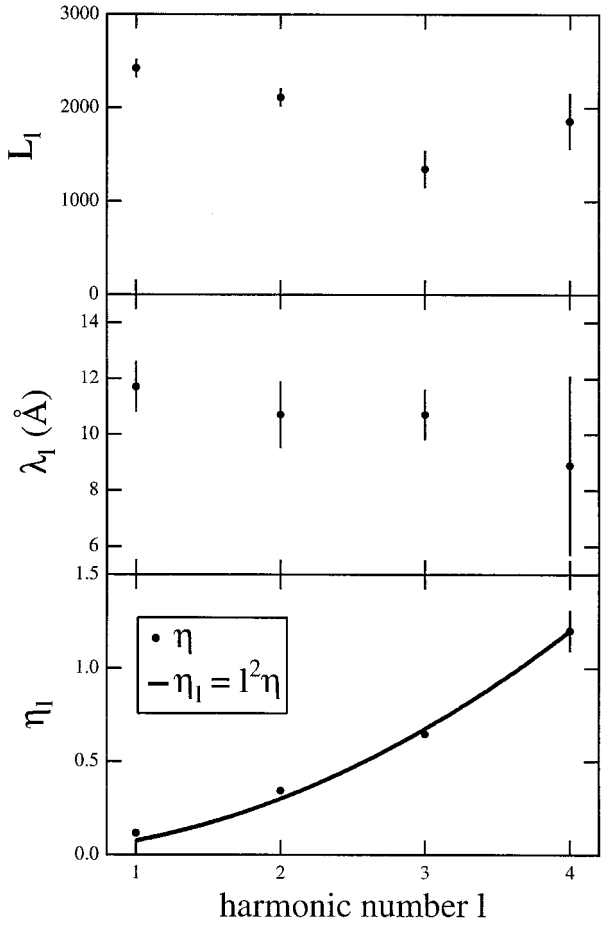

FIGURE 13 Fit parameters for the sample of Figs. 12 *D* and 9, III *H* plotted as a function of harmonic *l*. Plots of domain size *L* and peak asymmetry λ show little variation with harmonic order. However, the power law exponent η_l versus harmonic number shows the l^2 behavior expected for a material governed by the Landau-DeGennes Hamiltonian (Eq. 15).

in Fig. 18 *A* are generally consistent with this picture. Both photos show primarily black areas indicating that a homeotropic (lamellae parallel to the glass surfaces of the capillary) alignment dominates. As seen on a much smaller scale in the electron microscopy photos, the well-aligned areas are occasionally broken by large defects. In the polarization photos, the most common defects are isolated "oily streaks," a characteristic of lamellar phases with melted chains. A basic model of the oily streak as a disinclination pair (Asher and Pershan, 1979; Schneider and Webb, 1984), each part of strength $+1/2$, is shown in Fig. 19 *A*. Striations along the length of the defect (*z* axis) can be attributed to undulations of the defect axis in and out of alignment with the axes of

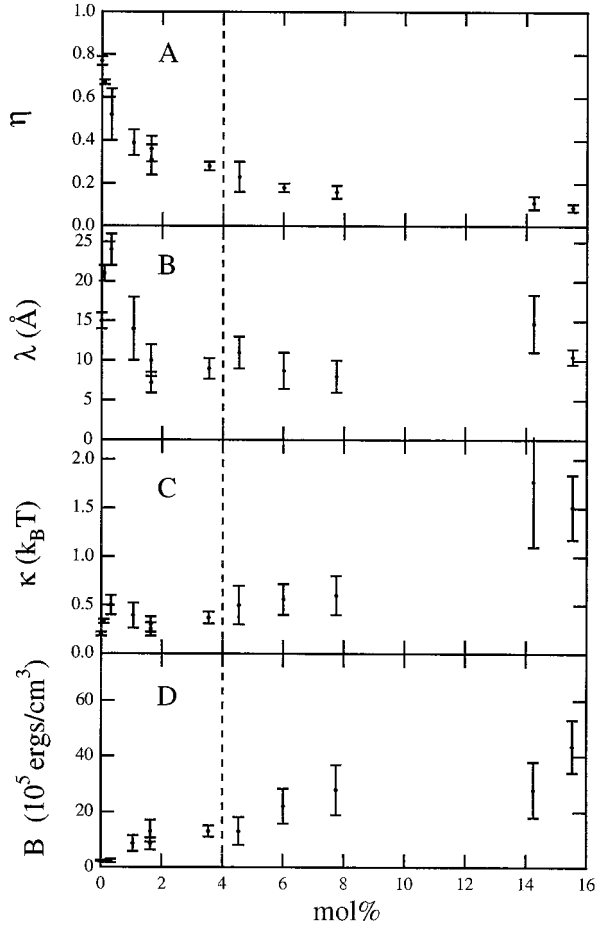

FIGURE 14 Fit parameters and calculated elasticity constants for 12 samples with increasing PEG2000 concentration that span the L_α-$L_{\alpha,g}$ transition (*dotted line*). For this set of samples, water concentration is approximately constant ($\Phi_w \sim 0.75$, $d = 140 \pm 15$ Å) while $c_{PEG2000}$ increases from 0 to 15.6 mol %. For all four parameters, there is no discontinuity at the fluid-gel transition. (*A*) The power law exponent η smoothly decreases as the PEG2000 concentration increases, indicating a change in the product $B\kappa$. (*B*) λ also generally decreases as $c_{PEG2000}$ increases, reflecting the increase in peak asymmetry. Since $\lambda \sim B^{-1/2}$, this trend implies the growth in the compressional modulus seen in (*D*). The data for λ are not as smooth as for η, reflecting the greater difficulty in obtaining reliable estimates for λ from peak asymmetry. (*C*) Single-membrane bending rigidity as a function of $c_{PEG2000}$. Within the accuracy of our measurements, bending rigidity is basically unchanged until $c_{PEG2000} \sim c_{mono}$ at ~8 mol %. (*D*) Bulk compressional modulus B versus PEG-DMPE concentration. The increase in B at low PEG-DMPE coverages where κ is constant indicates that the interaction between the bilayers is not purely a Helfrich undulation repulsion.

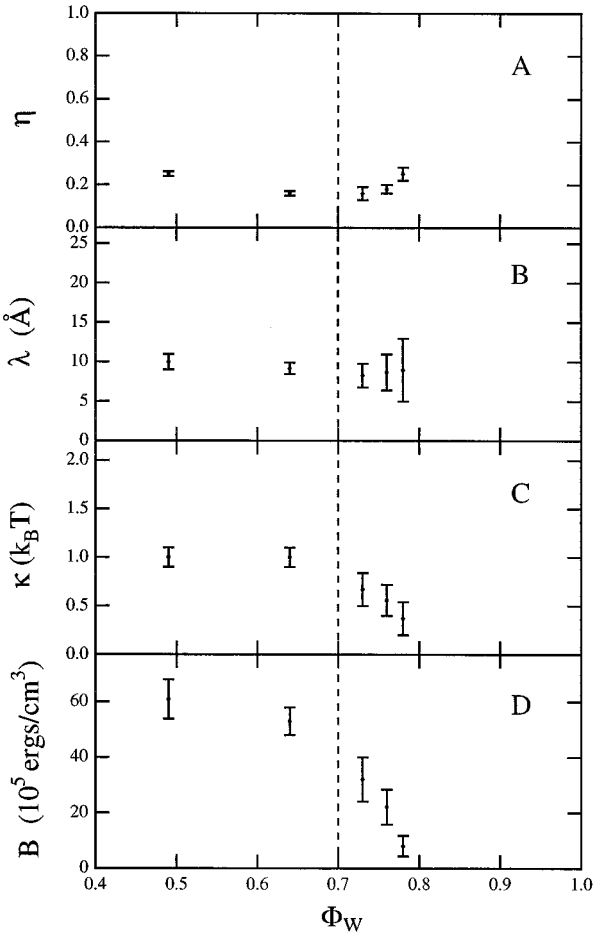

FIGURE 15 Fit parameters and calculated elasticity constants for five PEG2000 samples that span the L_α-$L_{\alpha,g}$ transition (*dotted line*). For this set of samples, Φ_w increases while $c_{PEG2000}$ is fixed at 6.05 ± 0.04 mol %. For all parameters, there is no discontinuity at the fluid-gel transition. (*A*) With the exception of the first point, the power law exponent η slowly increases with water concentration, reflecting the expected inverse d dependence of $B\kappa$. For the first point, $d \sim 25$ Å, low enough that hydration and van der Waals interactions are still important, making interpretation of η difficult. (*B*) λ, within the precision of our measurements, is flat. Given that $\lambda \sim (\kappa/B)^{1/2}$, and that B is expected to decrease with intermembrane distance or Φ_w much more quickly than κ, this is a surprising result. As in Fig. 14, the data for λ are not as smooth as for η, reflecting the greater difficulty in reliably determining peak asymmetry than in measuring a power law decay. (*C*) Single-membrane bending rigidity as a function of Φ_w. With the exception of the lowest water concentration data point, κ shows the logarithmic decrease with d_w expected for a flexible bilayer. It is unlikely that this trend is associated with the fluid-gel transition since, in Fig. 14, κ grows after the transition point. (*D*) The bulk compressional modulus B is a smoothly decreasing function of Φ_w (or d). Comparing the trend here with that in Fig. 14 *D*, we conclude that changes in the bulk compressional modulus are not correlated with the viscoelastic transition.

the crossed polarizers. The defect structure can also be described in terms of two opposite edge dislocations (Kleman, 1983).

The textures of samples near the L_α-$L_{\alpha,g}$ transition are strikingly different. As the transition to the $L_{\alpha,g}$ region is approached, the defect density rises sharply (Fig. 17, *A* and *B*; Fig. 18 *B*). In the optical microscopy photos, line defects proliferate and thin, acquiring a wispy appearance (e.g., Fig. 17 *F*, *arrow*). A more detailed freeze-fracture and optical microscopy study (Keller et al., 1997) showed that the microstructure changes at the transition from flat, well-aligned layers to a high density of spherulitic (Fig. 17 *B*) and cylindrical defects. Strikingly, shared membranes, like those highlighted by the star in 17 *B*, tether the defects together. Although isotropic spherulites are a common observation in both freeze-fracture and polarization microscopy of MLVs (Fig. 17, *D* and *H*), tethering membranes are

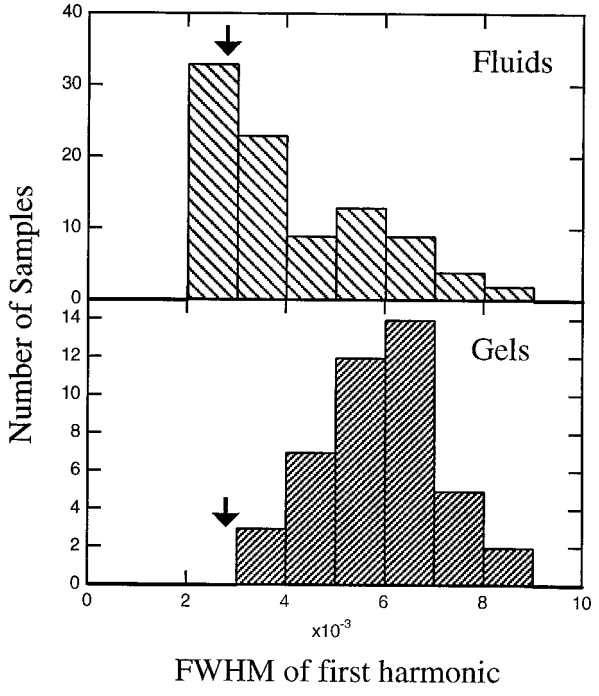

FIGURE 16 Histograms of first harmonic FWHM taken from synchrotron x-ray-scattering data of PEG2000 and PEG5000 samples (analagous data for PEG550 was not collected). The arrow indicates spectrometer resolution. (*Top*) Histogram of the first harmonic peakwidths for PEG2000 and PEG5000 fluid samples. Note that over one-third of these scans were resolution-limited. (*Bottom*) Histogram of the first harmonic peakwidths for gel samples. Almost none of these peaks were resolution-limited, indicating a much smaller average domain size than found in the fluid samples. The probability that the two histograms are drawn from the same distribution is $<1.6 \cdot 10^{-8}$ (Kolmogorov-Smirnov statistic).

not, as illustrated by the photo in Fig. 17 *D* of DDAB MLVs in water. Much of the viscoelastic response of the $L_{\alpha,g}$ could be due to this network of membrane links.

Deeper within the $L_{\alpha,g}$ regime, the defect density continues to increase and the size of the individual defect drops. Spherulites, polydisperse and often anisotropic, are the most common texture in freeze-fracture photos (Fig. 17 *C*, *arrow*), although cylindrical defects have also been observed (Keller et al., 1997). Well-aligned areas of parallel membranes are rare. In optical microscopy, the wispy texture remains a common textural observation; additionally, regions of densely packed and highly aligned defects (Figs. 17 *G* and 18 *C*) provide evidence of what appears to be a longer-range ordering of defects. A cut through a gel or transition sample similar to the cut shown in 19 *A* might appear as shown schematically in Fig. 19 *B*: a dense packing of edge dislocation pairs and spherulitic or quasispherulitic defects. The core of a spherulitic and an ellipsoidal defect are magnified to depict PEG-DMPE aggregated in the more curved regions of the membrane surface. Anisotropic molecules are expected to aggregate in regions satisfying their spontaneous curvature; for PEG-DMPE, these are the positive curvature regions. At the high water content limit of the $L_{\alpha,g}$ regime, the gel dissolves again to a fluid (e.g., Fig. 5, top test tube) and the optical texture changes to show large MLVs coexisting with oily streaks (Fig. 18 *D*).

It has been shown theoretically and experimentally that introducing defects can increase the effective viscoelasticity of anisotropic (lamellar) samples (Kawasaki and Onuki, 1990; Larson et al., 1993; Lu and Cates, 1994; Panizza et al., 1996). However, in previous studies, this effect has been transitory since the defects tended to relax away quickly, returning the sample to a relatively well-ordered state and a more liquid-like viscoelastic response (Larson et al., 1993; Panizza et al., 1996). In contrast, defects in the $L_{\alpha,g}$ appear to be stable over time and a consistent, gel-like response is maintained for years. Warriner et al. postulated that in the $L_{\alpha,g}$, PEG-DMPE aggregates in and stabilizes high-curvature, defected regions; as in the more transitory lamellar gels cited above, the macroscopically interacting defects collectively resist shear, giving rise to strong elasticity.

Attempts to anneal defects in the fluid phase are generally successful, indicating that the flat bilayer is the lowest energy state of the L_{α} regime. In contrast, gel samples defy both temperature and shear annealing. As the transition region is approached from the fluid regime, the melting temperature increases from the ~40°C required for L_{α} samples to >120°C (Warriner, 1997). At these elevated temperatures, polarization microscopy observations show that samples tend to cavitate and phase separate, preventing effective annealing. However, the temperature-induced transition from $L_{\alpha,g}$ to isotropic liquid is reversible; in several experiments in which we monitored the lamellar peak position as we melted and recooled the sample, we found no change in the repeat spacing and no change in sample mosaicism (i.e., no increase in alignment).

In some samples, we avoided cavitation of the sample by remaining just below the cavitation temperature; however, many defects remained at the end of even 24-h equilibrations, providing nucleation sites for vast defect networks during cooling. The most common texture found after annealing was the polygonal defect array—densely packed, intersecting parabolas with vertices at different levels in the sample. Even areas that initially appeared free of defects just after annealing tended to rapidly renucleate such arrays. Moreover, the high temperatures and long equilibration times required to influence the defect density virtually guarantee an appreciable amount of sample degradation in lipid samples (Schneider and Webb, 1984).

Shear annealing, done with a homemade apparatus of two glass plates separated by ~100 μm and frequencies of 1–10 Hz, was similarly ineffective in removing the defects from gel samples. Defects in fluid samples, in contrast, were routinely removed by moderate shear. This is not really surprising, given the previously described rheology data for gel and fluid samples. The resistance of the gel to both types of annealing, the longevity and overwhelming predominance of defects observed in polarization and freeze-fracture images, and the marked reduction in the average domain size observed in x-ray scattering from $L_{\alpha,g}$ samples,

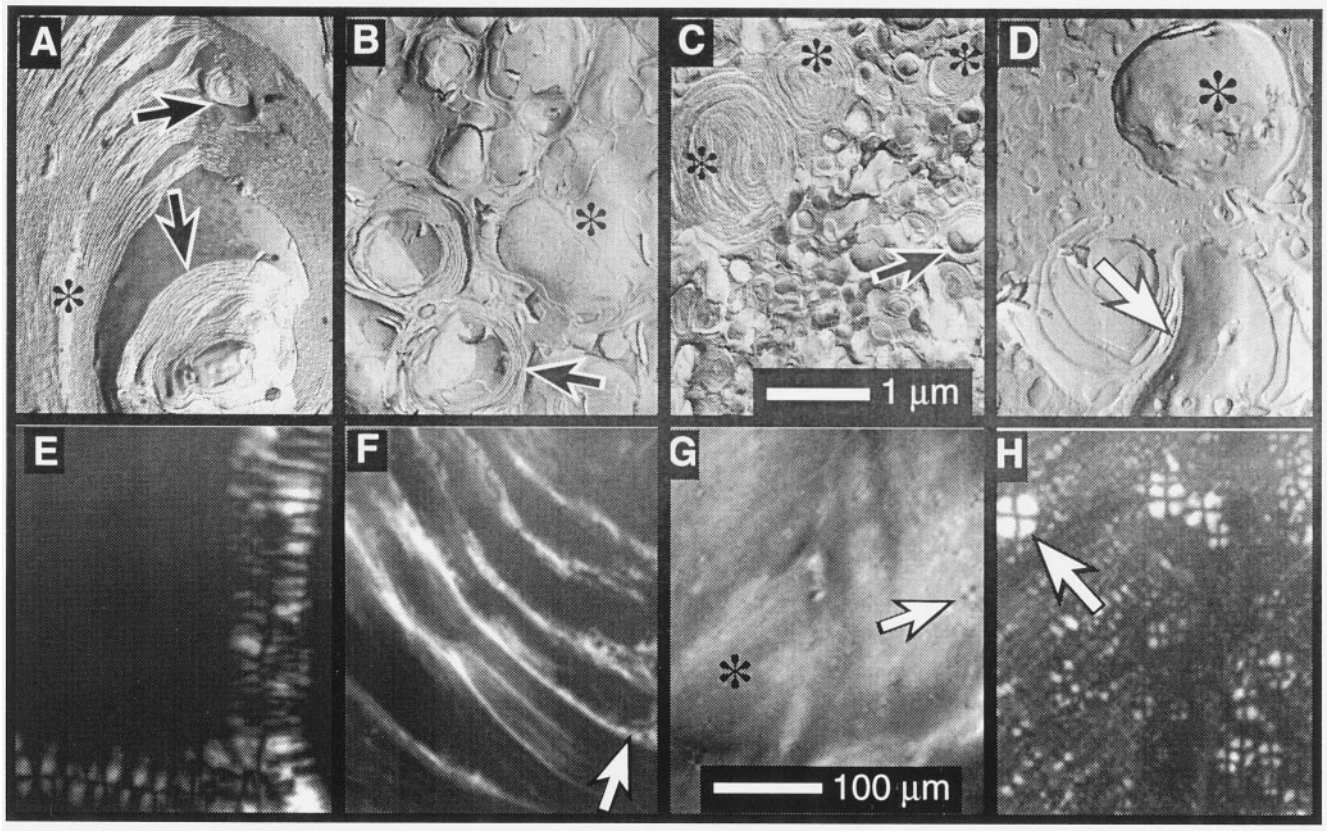

FIGURE 17 Freeze-fracture electron microscopy and polarizing optical microscopy data along a line of increasing $c_{PEG2000}$. The photos of *D* and *H* are of a suspension of MLVs made of DDAB and are included for comparison. All photos are reprinted with permission from Physical Review Letters (Keller et al., 1997). The upper images show typical morphologies observed by electron microscopy. Panels *A–D* have the same scale. Optical micrographs produced under crossed polarizers appear in the lower images (*E–H*) and all have the same scale. (*A*) Fluid sample, $c_{PEG2000} = 0.30$, $\Phi_w = 0.80$, $d = 155$ Å; well-ordered lamellae (*star*) and few defects (*arrows*). (*E*) Same sample: vertical and horizontal "oily streaks" against a background devoid of defects. (*B*) Sample near the fluid-gel transition with $c_{PEG2000} = 4.19$, $\Phi_w = 0.77$, $d = 147$ Å: curved regions of spherulite defects (*arrow*) interconnected by membranes (*star*). (*F*) Same sample as (*B*): the defect density has clearly increased but the size of individual defects shrinks. (*C*) Gel sample with $c_{PEG2000} = 7.7$, $\Phi_w = 0.81$, $d = 188$ Å: smaller spherulites (*arrow*) and spherulites whose interior membranes are bent into crescents (*starts*). (*G*) Same sample as (*C*): sheet-like texture (*star*), and extinction crosses (*arrow*). (*D*) Electron micrograph of multilamellar vesicles (MLVs) of DDAB that are not connected by membranes. Some vesicles are spherical (*star*) while others have anisotropic shapes such as crescents (*arrow*). (*H*) Optical micrograph of a 95% water suspension of DDAB MLVs showing extinction crosses (*arrow*). The predominance of spherically symmetric extinction crosses in the polarizing microscopy data indicates that for the DDAB suspension, anisotropic shapes are rare. Note that the data do not indicate this for defects in the gel phase (*C* and *G*).

lead us to believe that the flat bilayer may not be the lowest energy state for these lamellar gels.

DISCUSSION AND MODEL

A model of the lamellar fluid-gel transition has been proposed based on a softening of the free energy of line defects (Warriner et al., 1996). This model is qualitatively consistent with the experimentally observed proliferation of defects and increase in x-ray diffraction peak widths near the L_α-$L_{\alpha,g}$ transition. It also predicts the observed inverse relationship between water concentration (or intermembrane distance d) and PEG-DMPE concentration along the gel line expressed in Eqs. 10 and 11. In addition, the model predicts that the position of the fluid-gel transition depends on the molecular weight of the PEG moiety of the polymer-lipid. As the three PEG-DMPEs in this study span an order of magnitude in molecular weight, we are in a good position to quantitatively check this dependence. The only adjustable parameter in the gelation model is the membrane bending elasticity κ; we thus check the model by comparing the value for κ obtained here with that calculated via the Caille lineshape analysis in the x-ray section.

We briefly review the model here. The cost of defect formation is set by two phenomenological constants: the bending rigidity κ and the spontaneous membrane curvature C_0, both sensitive functions of membrane composition. We have shown that κ is unaffected at the concentrations where the $L_{\alpha,g}$ first appears, hence we can legitimately focus on C_0. The majority membrane components, DMPC and pentanol, have an effective natural radius of curvature $C_0^L = 0$ (Fig. 1, *top right*); this is demonstrated by the propensity to form large, homeotropically oriented samples in highly dilute lamellar phases of DMPC and pentanol. The PEG-

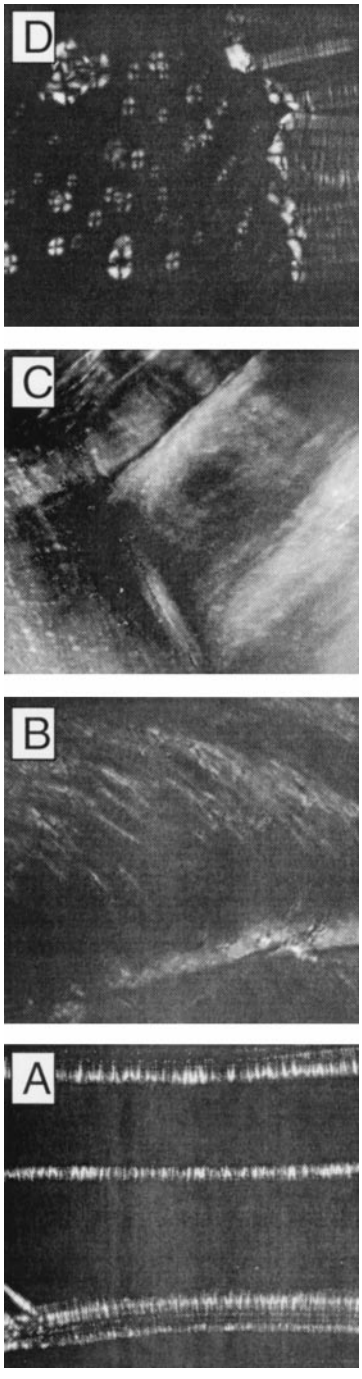

FIGURE 18 Polarizing optical microscopy photos of defects in PEG5000 samples along a line of increasing Φ_w. (*A*) Fluid, $c_{PEG5000} = 1.63$, $\Phi_w = 0.73$, $d = 122$ Å. Sample shows the "oily streak" defect typical of L_α phases. These defects can be annealed away. (*B*) Gel, $c_{PEG5000} = 1.50$, $\Phi_w = 0.84$, $d = 220$ Å. As seen in the increasing c_{PEG} line, the defect density increases while the size of the individual defects shrinks. Line defects in the $L_{\alpha,g}$ phase cannot be annealed. (*C*) Gel, $c_{PEG5000} = 1.47$, $\Phi_w = 0.83$ (*d* not measured). Disinclinations between highly defected regions become common, resulting in a white, "sheet-like" texture separated by dark brushes. (*D*) Two-phase, $c_{PEG5000} = 1.33$, $\Phi_w = 0.87$. In the presence of excess water, the gel phase separates into a lamellar phase plus excess solvent. These samples are characterized by roughly equal proportions of MLVs and oily streaks.

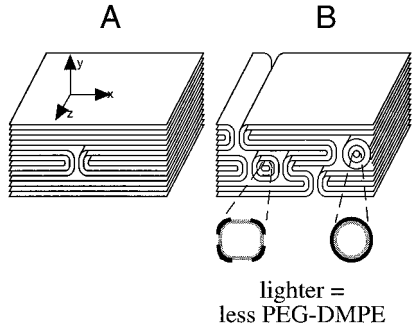

FIGURE 19 Real space structure attributed to the defects in the (*A*) fluid L_α and (*B*) gel $L_{\alpha,g}$ phases. (*A*) A single oily streak defect embedded in a large, well-aligned region. This oily streak, representative of focal conic defects of the first kind, is composed of a defect pair with opposite Burgers vectors of strength six. (*B*) Many oily streak defects interspersed with focal conic defects of the second kind. Well-aligned regions are rare. The two insets depict distributions of PEG-DMPE that would tend to help stabilize defects. On the left, PEG-DMPE aggregates in the more highly curved regions of an oblate cylinder, while on the right, PEG-DMPE has a higher concentration on the outside wall of a spherical defect.

DMPE component has a positive natural radius of curvature $C_0^P > 0$ (Fig. 1, *top right*). In particular, it is known to stabilize vesicles (Kenworthy et al., 1995). At low PEG-DMPE concentrations the two components may be uniformly mixed (Fig. 20, *top*). As the PEG-DMPE concentration increases, a frustration should develop in which the different components compete for optimal membrane curvature. The segregation of PEG-DMPE into stable edge dislocation defects would satisfy both components. Theoretical work has shown that a material with a non-zero natural radius of curvature in a multicomponent membrane should be "attracted" to regions satisfying that curvature (Leibler, 1986; Lipowsky, 1993). Defects as regions of high membrane curvature thus represent natural aggregation sites for the PEG-DMPE (Fig. 20, path ii and Fig. 19, magnification of an ellipsoidal defect).

Another, independent pathway to defect formation is also possible, based on inter-PEG attractive forces. In a lamellar system, in-plane phase separation could promote defect

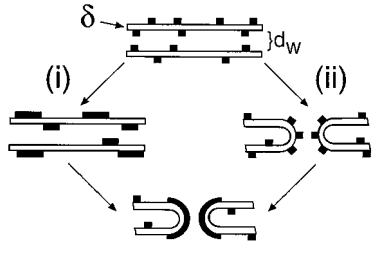

FIGURE 20 Cartoon of two possible defect formation paths. In (i) the PEG-lipid phase separates in the plane of the bilayer, forcing the formation of a curved region (defect) to accommodate the higher local spontaneous curvature of the polymer-lipids. In (ii) PEG-lipids remain uniformly dispersed across the bilayer until the formation of a defect "attracts" them to the curved region. In either case the PEG-lipids remain in and stabilize the regions of higher curvature.

formation. Phase separation has already been observed in PEG monolayers spread at an air-water interface (Cao and Kim, 1994). As depicted schematically in path i, Fig. 20, PEG-DMPE in the lamellar system might also undergo in-plane phase separation, creating a region of high spontaneous curvature and defect formation. Spherulitic defects, with a higher concentration of PEG-DMPE on the outer monolayer than the inner monolayer, would be one example of defects resulting from this mechanism (Fig. 19, magnification of a spherulite). Regardless of which path is taken, PEG-DMPEs should act to stabilize defects. In particular, the presence of PEG-DMPE should augment resistance to shearing forces that necessarily both reduce the intermembrane distance and tilt the bilayers, compressing the attached polymers. Tightly packed, interacting defects distributed throughout the sample would resist shear in all directions, creating a network with a gel-like elasticity. The tethering membranes detected in freeze-fracture electron microscopy would enhance this effect.

For ease of calculation, only the simplest defect is considered: a line formed by an edge dislocation pair of opposite Burgers vector 2 (Fig. 20, *bottom*). The elastic cost of forming any defect is given by the Helfrich elastic energy of fluid membranes (Helfrich, 1978)

$$E = \frac{1}{2}\kappa \int [(C_1 - C_0) + (C_2 - C_0)]^2 dS \qquad (25)$$

where C_0 is the spontaneous radius of curvature.

The principal curvatures of the line defect pictured in Fig. 21 are $C_1 = 2/d$ and $C_2 = 0$, which lead to:

$$E = \frac{1}{2}\kappa\left(\frac{2}{d} - C_0\right)^2 \pi L d \qquad (26)$$

where L is the length of the defect. A line defect has a persistence length ξ_p along its main axis given by (F. MacKintosh, private communication)

$$\xi_p = \frac{\pi d \kappa}{k_B T} \qquad (27)$$

The entropic contribution to the free energy is therefore

$$TS = \frac{(k_B T)^2 L}{\pi d \kappa} \qquad (28)$$

At the defect proliferation/gelation point, the elastic cost will equal the entropic gain. Equating Eqs. 26 and 28 and solving for d then gives

$$d_{gel} = \frac{1}{C_{0_{gel}}}\left(2 - \frac{\sqrt{2}k_B T}{\pi\kappa}\right) \qquad (29)$$

In the above expression, C_0 can be estimated as the sum of the curvatures of the different membrane components. This mean-field type of expression is only valid for noninteracting PEG-DMPEs—i.e., for concentrations $c_{PEG} \ll c_{mono}$ so that each PEG-DMPE acts independently. Since C_0 for both DMPC and pentanol is zero, the C_0 of the membrane is proportional to the product of C_0^P and the global volume fraction of PEG-surfactant in the membrane, $\Phi_{mem_{PEG}}$. Thus the relationship between the lamellar spacing d_{gel} and PEG-DMPE concentration $\Phi_{mem_{PEG}}$ along the gelation line finally reads

$$d_{gel} = \frac{2 - \frac{\sqrt{2}k_B T}{\pi\kappa}}{\phi_{mem_{PEG}} C_0^P} \qquad (30)$$

Since $\Phi_{mem_{PEG}}$ is roughly proportional to $N \cdot c_{PEG}$ and d is proportional to Φ_W, Eq. 30 implies that the fluid-gel tran-

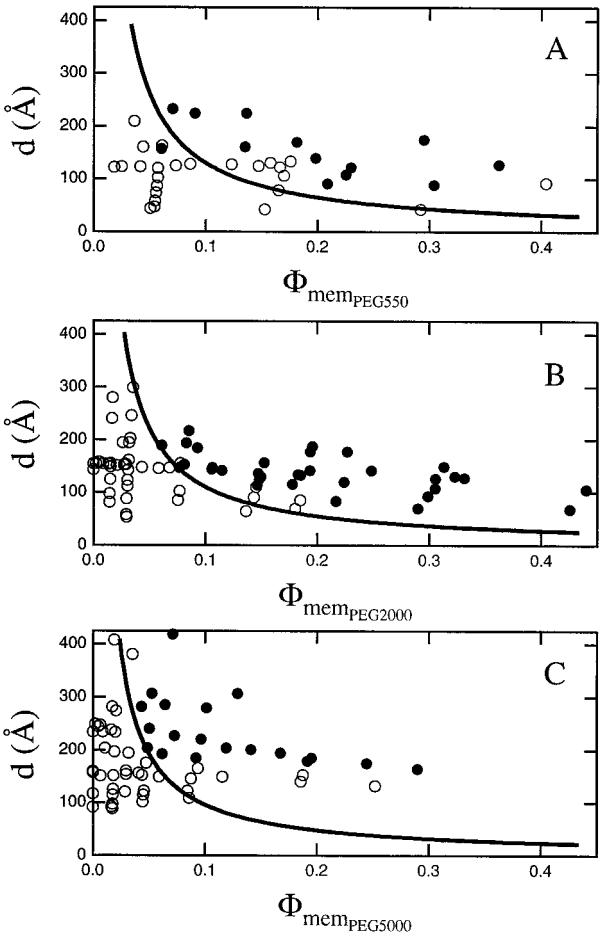

FIGURE 21 Fluid-gel transition curve plotted with data for PEG550 (*A*), PEG2000 (*B*), and PEG5000 (*C*). The model curve is the solid line; fluid points are open circles; gel points are solid circles. The model curve is a weighted least-squares fit to Eq. 29:

$$d_{gel} = \frac{m}{\phi_{mem_{PEG}}} \quad \text{where} \quad m = \frac{2 - (\sqrt{2}k_B T/\pi\kappa)}{C_0^P}$$

For PEG550, we obtained $m = 13.0 \pm 0.3$, for PEG2000, $m = 11.0 \pm 0.2$, and for PEG5000, $m = 9.6 \pm 0.2$. While the model curves agrees qualitatively with data, quantitative agreement is poor, especially at high volume fractions of PEG-lipid where the assumption of a dilute gas of PEG-lipids in the plane of the membrane breaks down. Reduced χ^2 values are: $\chi^2_{550} = 51$; $\chi^2_{2000} = 39$; $\chi^2_{5000} = 49$.

sition line obeys

$$\Phi_w \propto \frac{1}{c_{PEG}} \tag{31}$$

These results are qualitatively consistent with the phase diagrams of Figs. 3 and 4. Remarkably, this simple model contains the observed inverse relationship between water and polymer content required for gelation (or d and $\Phi_{mem_{PEG}}$). It is also possible to extract the dependence on the polymer polymerization number N by regarding the PEG-DMPEs as highly asymmetric diblock copolymers. The spontaneous curvature of an asymmetric block copolymer located on a spherical vesicle interface is calculated to be (Wang and Safran, 1990)

$$C_0^P = \frac{2\epsilon\pi^{2/3}a^2}{12^{1/3}(1+3\epsilon^2)N^{2/3}\chi^{1/6}v} \tag{32}$$

where ϵ, an asymmetry parameter, is 1/2 − (phobic length/total length); a, v are the length and volume of a PEG monomer, respectively, and χ is the Flory-Huggins parameter for PEG in water. Thus $C_0^P \propto 1/N^{2/3}$, which leads to the scaling law $\Phi_{w_{gel}} \propto 1/N^{1/3}$. This is the correct qualitative trend in the scaling behavior of the PEG-DMPE systems: in particular, it implies that larger polymer-lipids induce gelation at lower Φ_W or lower c_{PEG} than smaller polymer lipids, as observed.

To quantitatively check the agreement between this model and our phase data, we calculate transition points by taking the average of d and $\Phi_{mem_{PEG}}$ for the fluid and gel samples nearest the transition. That is,

$$d_{gel} = \frac{(d_{L_{\alpha,g}} + d_{L_\alpha})}{2}$$

$$\Phi_{mem_{gel}} = \frac{(\Phi_{L_{\alpha,g}} + \Phi_{L_\alpha})}{2} \tag{33}$$

$$\delta d_{gel} = \frac{1}{2}\sqrt{\delta d_{L_{\alpha,g}}^2 + \delta d_{L_\alpha}^2 + (d_{L_{\alpha,g}} - d_{L_\alpha})^2}$$

We then perform a weighted least-squares fit to the expression $d = m/\Phi_{mem_{PEG}}$ where $m = 2 - (\sqrt{2}k_BT/\kappa)/C_0^P$ is the fitted parameter. Fig. 21 shows the fitted model curves plotted with d versus $\Phi_{mem_{PEG}}$ data for each of the PEG-DMPEs. Agreement is clearly best for the lower values of $\Phi_{mem_{PEG}}$, where the assumption of a noninteracting gas of PEG-DMPEs is valid. By eye the fits seem to worsen with increasing polymer size, but reduced χ^2 values are actually very similar for all three molecular weights. The lack of good quantitative agreement is not surprising. For example, the previously discussed ambiguity in the method used to classify fluid and gel samples tends to increase the error in identifying transition points, necessarily increasing the reduced χ^2. Additionally, the model itself is over-simplified; a more complete model, taking into account both the lower stability limit in the phase diagram and the many other defect geometries observed in the $L_{\alpha,g}$ structure, would doubtless have more success. However, the model does produce the correct general relationship between Φ_W and c_{PEG} at the transition and even allows reasonable estimates of the membrane bending rigidity κ. Taking

χ = 0.23 (Bae et al., 1993)
v ≅ 57 Å^3 (Berry and Fox, 1968; Dee et al., 1992)
$a \equiv v^{1/3}$

and

$$\epsilon = \frac{1}{2} - \frac{\delta/2}{\delta/2 + R_g}; \quad \epsilon_{550} = 0.49; \quad \epsilon_{2000} = 0.32;$$

$$\epsilon_{5000} = 0.19$$

in the C_0^P calculation of Eq. 33, one finds a natural radius of curvature for PEG550 of ~350 Å, and 190 Å for the two larger PEG-DMPEs. Inserting this value into the expected slope for the three transition curves (Eq. 30) and comparing with the measured slopes, we obtain, for all the PEG-surfactant systems, a κ of ~0.3 k_BT at the viscoelastic transition. From the lineshape analysis (Fig. 14 *C*), this is indeed the correct value. Thus, this naive model yields a reasonable value of a relatively sensitive material constant.

As a last point we discuss the probable generality of the $L_{\alpha,g}$ phase. Our model suggests that a prerequisite for this type of gel is a low bending rigidity ($\kappa \sim k_BT$) for the individual membranes making up the L_α stacks. For larger values of κ, the intermembrane distance at which gelation begins will approach a limiting value (from Eq. 30):

$$d_{gel} \sim \frac{2}{C_0^P \Phi_{mem_{PEG}}} \tag{34}$$

Substituting, for example, our values for the PEG550 and PEG2000–PEG5000 C_0^P we obtain that gelation in the PEG2000–50000 case would occur only for $d \geq 400$ Å, and in the PEG550 case for $d \geq 700$ Å. Typically maximum intermembrane spacings in rigid L_α phases are below 100 Å. Thus, for most L_α phases, phase separation will obtain before gelation. We note that the $L_{\alpha,g}$ has not been reported in a very comprehensive study of polymer-decorated L_α membranes based on stiffer membranes (Kenworthy et al., 1995), nor have we seen the $L_{\alpha,g}$ in our own experiments using PEG-lipids in more rigid L_α phases.

CONCLUSION

We investigated three molecular weights of PEG-DMPE which, incorporated into fluid, extremely flexible membranes, yield a lamellar hydrogel phase, called $L_{\alpha,g}$. Larger molecular weight polymer-lipids form the gel at lower PEG-DMPE concentrations, showing that polymer molecular weight plays a deciding role in the L_α-$L_{\alpha,g}$ transition. Phase diagrams for the three PEG-DMPEs are qualitatively very similar, showing an inverse relationship between water concentration (d-spacing) and mol % ($\Phi_{mem_{PEG}}$) required to

form the gel. This behavior immediately distinguishes the $L_{\alpha,g}$ from more traditional polymer gels based on entanglements.

Small-angle x-ray scattering shows that samples remain lamellar regardless of PEG-DMPE molecular weight or sample viscoelasticity. A quantitative analysis of high-resolution spectra shows that the addition of PEG-DMPE to flexible lamellae leads to growth in the membrane bending elasticity only at concentrations exceeding monolayer coverage. However, PEG-DMPE also yields an increased intermembrane repulsion at much lower concentrations, described neither by the Helfrich undulation theory nor the mushroom-brush theory of grafted polymers. It is also clear that this interaction is merely incidental to the fluid-gel transition. High-angle x-ray scattering profiles demonstrate that in-plane lipid chain ordering is likewise absent in both fluid and gel samples. Moreover, electrostatic interactions do not play a role.

Small-angle x-ray data show that the average domain size of gel samples is consistently reduced from that of fluid samples. Polarized optical and freeze-fracture electron microscopy observations confirm this trend, revealing that a proliferation of "tethered" defects is associated with the gel transition. X-ray and polarizing microscopy temperature annealing experiments also argue that a high defect density is intrinsic to the gel phase. Rheometric measurements tend to confirm these observations while demonstrating the strong elasticity of the $L_{\alpha,g}$. We infer that the asymmetric PEG-DMPE molecule significantly increases the membrane spontaneous curvature. Preferring high-curvature regions (defects), PEG-DMPE both aggregates to existing defects and promotes a highly defected microstructure. Since domains with a layer normally along the direction of flow must resist shear, the random orientation of domains leads to the observed elasticity of the gel phase.

A model of channel defects created by the lateral phase separation of PEG-DMPE into defect-concentrated regions of the membranes predicts both the inverse relationship between Φ_W and c_{PEG} observed along the gel transition line and the scaling dependence of the interlayer spacing at the gel transition with PEG molecular weight. Remarkably, the model also provides an estimate of the bending rigidity of a single membrane which is in excellent agreement with the value obtained through quantitative fits to the scattering from samples near the L_α-$L_{\alpha,g}$ transition. However, the model does not describe the viscoelastic transition in detail, yielding reduced χ^2 values between 40 and 50.

We thank P. Pincus for useful discussions and insight. We also thank G. Subramanian for the preparation of DDAB vesicles used in the microscopy section of this paper.

This work was partially supported by National Science Foundation Grant DMR-9624091 and the Petroleum Research Fund (31352-AC7). J. A. Zasadzinski was supported by National Science Foundation Grant 9319447. S. L. Keller was supported by a University of California President's postdoctoral fellowship. The Materials Research Laboratory at Santa Barbara is supported by National Science Foundation Grant DMR-96-32716. Synchrotron Experiments were carried out at Stanford (SSRL) which is supported under the United States Department of Energy.

REFERENCES

Alexander, S. 1977. Polymer adsorption on small spheres: a scaling approach. *Journal de Physique.* 38:977–981.

Allen, T. M., and A. Chonn. 1987. Large unilamellar liposomes with low uptake into the reticuloendothelial system. *FEBS Lett.* 223:42.

Als-Nielsen, J., J. D. Litster, R. J. Birgeneau, M. Kaplan, C. R. Safinya, A. Lindegaard-Andersen, and S. Mathiesen. 1980. Observation of algebraic decay of positional order in a smectic liquid crystal. *Phys. Rev. B.* 22:312–320.

Asher, S. A., and P. S. Pershan. 1979. Alignment and defect structures in oriented phosphatidylcholine multilayers. *Biophys. J.* 27:393–421.

Bae, Y. C., J. J. Shim, D. S. Soane, and J. M. Prausnitz. 1993. Representation of vapor-liquid and liquid-liquid equilibria for binary systems containing polymers: applicability of an extended Flory-Huggins equation. *J. Appl. Polym. Sci.* 47:1193–1206.

Berry, G. C., and T. G. Fox. 1968. The viscosity of polymers and their concentrated solutions. *Adv. Polym. Sci.* 5:261.

Caille, A. 1972. Remarks on the scattering of x-rays by A-type smectics. *Comptes Rendus Hebdomadaires des Seances de l'Academie des Sciences, Serie B.* 274:891–893.

Cao, B. H., and M. W. Kim. 1994. Molecular weight dependence of the surface tension of aqeous poly(ethylene oxide) solutions. *Faraday Discussions.* 98:245–252.

Chiruvolu, S., E. Naranjo, and J. A. Zasadzinski. 1994. Microstructure of Complex Fluids by Electron Microscopy. C. A. Herb and R. K. Prud'homme, editors. American Chemical Society, Washington, DC. 118–138.

Dee, G. T., T. Ougizawa, and D. J. Walsh. 1992. The pressure volume temperature properties of polyethylene, poly(dimethyl siloxane), poly(ethylene glycol), and poly(propylene glycol) as a function of molecular weight. *Polymer.* 33:3462–3469.

DeGennes, P.-G. 1976. Scaling theory of polymer adsorption. *Journal de Physique.* 37:1445–1452.

DeGennes, P.-G. 1980. Conformation of polymers attached to an interface. *Macromolecules.* 13:1069–1071.

Demus, D., and L. Richter. 1978. Textures of Liquid Crystals. Weinheim, New York.

Fetter, R., and M. Costello. 1986. A procedure for obtaining complimentary replicas of ultra-rapidly frozen sandwiched samples. *J. Microsc.* 141:277–290.

Gonzalez-Tello, P., F. Camacho, and G. Blazquez. 1994. Density and viscosity of concentrated aqueous solutions of poly(ethylene glycol). *J. Chem. Engin. Data.* 39:611–614.

Gray, G. W., and J. W. G. Goodby. 1984. Smectic Liquid Crystals: Textures and Structures. Leonard Hill, Philadelphia.

Gunther, L., Y. Imry, and J. Lajzerowicz. 1980. X-ray scattering in smectic-A liquid crystals. *Phys. Rev. A.* 22:1733–1740.

Helfrich, W. 1978. Steric interactions of fluid membranes in multilayer systems. *Z. Naturforsch A.* 33:305–315.

Kawasaki, K., and A. Onuki. 1990. Dynamics and rheology of diblock copolymers quenched into microphase-separated states. *Phys. Rev. A.* 42:3664–3666.

Keller, E. N., D. Davidov, and C. Boeffel. 1991. Algebraic dependence of the structure factor and possible anharmonicity in a high-resolution x-ray study of a side-group polymeric liquid crystal. *Phys. Rev. A.* 43: 2897–2902.

Keller, S. L., H. E. Warriner, C. R. Safinya, and Z. A. N. Zasadzinski. 1997. Direct observation of a defect-mediated viscoelastic transition in a hydrogel of lipid membranes and polymer lipids. *Phys. Rev. Lett.* 78:4781–4784.

Kenworthy, A. K., K. Hristova, D. Needham, and T. J. McIntosh. 1995. Structure and phase behavior of lipid suspensions containing phospholipids with covalently attached poly(ethylene glycol). *Biophys. J.* 68: 1903–1921.

Kleman, M. 1983. Points, lines and walls. In Liquid Crystals, Magnetic Systems and Various Ordered Media. J. Wiley, New York.

Kuhl, T. L., D. E. Leckband, D. D. Lasic, and J. N. Israelachvili. 1994. Modulation of interaction forces between bilayers exposing short-chained ethylene oxide headgroups. *Biophys. J.* 66:1479–1488.

Landau, L. D. 1965. Collected Papers of L. D. Landau. Gordon and Breach, New York.

Larson, R. G., K. I. Winey, S. S. Patel, H. Watanabe, and R. Bruinsma. 1993. The rheology of layered liquids: lamellar block copolymers and smectic liquid crystals. *Rheologica Acta.* 32:245–253.

Lasic, D. D. 1993. Liposomes: From Physics to Applications. Elsevier, New York.

Lasic, D. D., and F. J. Martin, editors. 1995. Stealth Liposomes. CRC Press, Boca Raton, FL. 289.

Lasic, D. D., and D. Papahadjopoulos. 1995. Liposomes revisited. *Science.* 267:1275–1276.

Lee, V. H., editor. 1991. Peptide and Protein Drug Delivery. Marcel Dekker, New York. 891.

Lei, N., C. R. Safinya, and R. F. Bruinsma. 1995. Discrete harmonic model for stacked membranes—theory and experiment. *Journal de Physique II.* 5:1155–1163.

Leibler, S. 1986. Curvature instability in membranes. *Journal de Physique.* 47:507–516.

Lipowsky, R. 1993. Domain-induced budding of fluid membranes. *Biophys. J.* 64:1133–1138.

Lu, C.-Y. D., and M. E. Cates. 1994. Viscoelasticity of lyotropic smectics. *J. Chem. Phys.* 101:5219–5228.

Needham, D., T. J. McIntosh, and D. D. Lasic. 1992. Repulsive interactions and mechanical stability of polymer-grafted lipid membranes. *Biochim. Biophys. Acta.* 1108:40–48.

Panizza, P., D. Roux, V. Vuillaume, C.-Y. D. Lu, and M. E. Cates. 1996. Viscoelasticity of the onion phase. *Langmuir.* 12:248–252.

Peppas, N. A., and R. Langer. 1994. New challenges in biomaterials. *Science.* 263:1715–1720.

Reiss-Husson, F. 1967. Structure des phases liquide-crystalline de differents phospholipides, monoglycerides, sphingolipides, anhydres ou en presence d'eau. *J. Mol. Biol.* 25:363–382.

Roux, D., and C. R. Safinya. 1988. A synchrotron x-ray study of competing undulation and electrostatic interlayer interactions in fluid multimembrane lyotropic phases. *J. Physique (France).* 49:307–318.

Safinya, C. R. 1989. Rigid and fluctuating surfaces: a series of synchrotron x-ray scattering studies of interacting stacked membranes. *In* NATO Advanced Study Institute on Phase Transitions in Soft Condensed Matter. T. Riste and D. Sherrington, editors. Plenum Publishing Corporation, New York. 249–269.

Safinya, C. R., D. Roux, G. S. Smith, S. K. Sinha, P. Dimon, N. A. Clark, and A. M. Bellocq. 1986. Steric interactions in a model multimembrane system: a synchrotron x-ray study. *Phys. Rev. Lett.* 57:2718–2721.

Safinya, C. R., E. B. Sirota, R. F. Bruinsma, C. Jeppesen, R. J. Plano, and L. J. Wenzel. 1993. Structure of membrane surfactant and liquid crystalline smectic lamellar phases under flow. *Science.* 261:588–591.

Safinya, C. R., E. B. Sirota, D. Roux, and G. S. Smith. 1989. Universality in interacting membranes: the effect of cosurfactants on the interfacial rigidity. *Phys. Rev. Lett.* 62:1134–1137.

Schneider, M. B., and W. W. Webb. 1984. Undulating paired disinclinations (oily streaks) in lyotropic liquid crystals. *Journal de Physique.* 45:273–281.

Small, D. M. 1986. The physical chemistry of lipids. *In* Handbook of Lipid Research. D. J. Hanahan, editor. Plenum Press, New York. 512.

Stephen, H., and E. Stephen, editors. 1963–1979. Solubilities of Inorganic and Organic Compounds. Pergamon Press, New York.

Trauble, H., and D. H. Haynes. 1971. The volume change in lipid bilayer lamellae at the crystalline-liquid crystalline transition. *Chem. Phys. Lipids.* 7:324.

Wang, Z. G., and S. Safran. 1990. Equilibrium emulsification of polymer blends by diblock copolymers. *Journal de Physique.* 51:185–200.

Warriner, H. E. 1997. X-ray Diffraction, Polarizing Optical Microscopy, and Rheological Studies of a Lamellar Gel Containing Polymer-Surfactants. University of California, Santa Barbara.

Warriner, H. E., P. Davidson, N. L. Slack, M. Schellhorn, P. Eiselt, S. H. J. Idziak, H.-W. Schmidt, and C. R. Safinya. 1997. Lamellar biogels comprising fluid membranes with a newly synthesized class of polyethylene glycol-surfactants. *J. Chem. Phys.* 107:3707–3722.

Warriner, H. E., S. H. J. Idziak, N. L. Slack, P. Davidson, and C. R. Safinya. 1996. Lamellar biogels: fluid-membrane based hydrogels containing polymer-lipids. *Science.* 271:969–973.